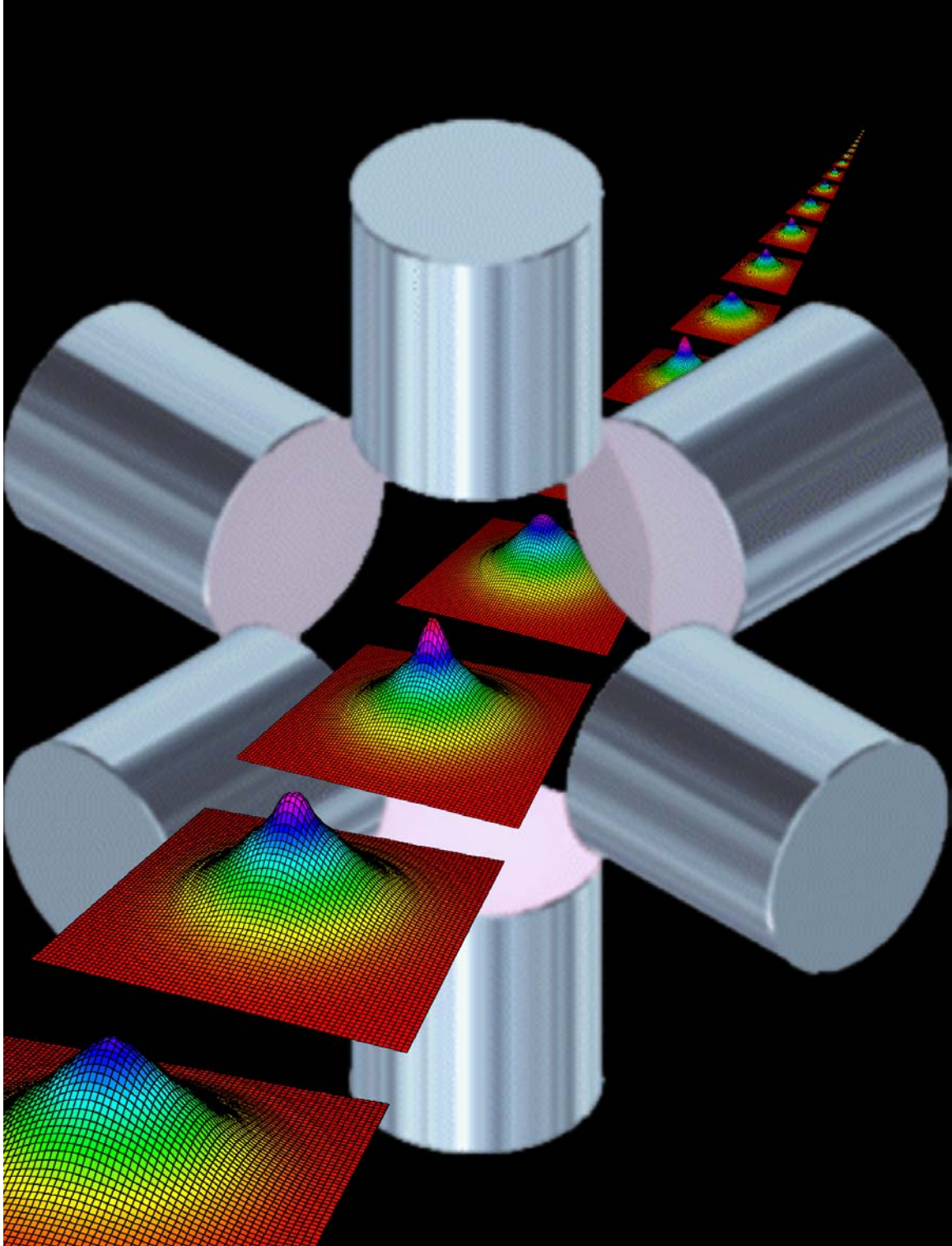


CHAPTER 2

LASER COOLED ATOMIC PHYSICS



Atom Interferometer Inertial Force Sensors

Jeff McGuirk, Dallin Durfee, Jeff Fixler, Greg Foster, Yoav Shaham and Mark Kasevich
Yale University

Recent advances in the field of atom interferometry have opened the possibility of a new class of precise and accurate inertial force sensors. We have built laboratory prototypes of gravimeters, gravity gradiometers and gyroscopes based on these principles. The corresponding demonstrated laboratory sensitivities for these instruments are $2 \times 10^{-9} \text{ g/Hz}^{1/2}$ (accelerometer), $4 \text{ E/Hz}^{1/2}$ (gravity gradiometer, $1 \text{ E} = 10^{-9} \text{ sec}^{-2}$) and $2 \times 10^{-6} \text{ deg/hr}^{1/2}$ (gyroscope) respectively. These ground-based instruments now perform at levels that meet or exceed other state-of-the-art sensors.

Our technical approach draws upon recent advances in the fields of atom interferometry and laser cooling, and is fundamentally different from other state-of-the-art instruments. First, the proof-masses used in our work are individual atoms rather than precisely machined macroscopic objects. This reduces systematic effects associated with the material properties of macroscopic objects. Second, their calibration is referenced to the wavelength of a frequency-stabilized laser. This provides long-term accuracy. Finally, our approach allows integration of multiple sensors into a single package with little change in overall instrument design.

We will review the underlying physical principles of these sensors, and discuss possible applications to microgravity science and technology. Fundamental physics applications include tests of the Equivalence Principle at the 10^{-16} g level, a search for spin-dependent gravitational forces, and other test of General Relativity. Technology applications include next generation sensors for satellite drag compensation, for advanced inertial navigation, and for geodesy.

A Quantum Degenerate Fermi Gas of ${}^6\text{Li}$ Atoms

Experiments with Quantum Gases of Lithium

J. M. Gerton, I. Prodan, D. Strekalov, W. I. McAlexander, K. Strecker, A. Truscott,
and R. G. Hulet
Physics Department, Rice University

Abstract

Lithium has two naturally occurring isotopes, ${}^6\text{Li}$ and ${}^7\text{Li}$, with opposite exchange symmetry. In this paper, we describe experiments with ultracold, trapped gases of the lithium isotopes. Molecular spectroscopy of a Bose-Einstein condensate of ${}^7\text{Li}$ has produced spectral linewidths of less than 250 Hz. This high spectral resolution enables the condensate to be selectively removed, without disturbing the non-condensed thermal atoms, and for the first time, to directly observe the growth and collapse of a condensate with attractive self-interactions. We also report progress towards the observation of a BCS phase transition in a gas of fermionic ${}^6\text{Li}$ atoms.

Introduction

Lithium is an attractive atom for investigations of the effects of quantum statistics because its two naturally occurring isotopes, ${}^6\text{Li}$ and ${}^7\text{Li}$, have opposite exchange symmetry. Since ${}^6\text{Li}$ is composed of an odd number of spin-2 particles (3 electrons, 3 protons, 3 neutrons), it is itself a half-integer composite particle obeying Fermi-Dirac statistics. On the other hand, ${}^7\text{Li}$ with its extra neutron is a composite boson. The phenomena exhibited by each isotope, therefore, should be vastly different at ultra-low temperatures, where effects of quantum degeneracy are manifested. For example, we have shown that ${}^7\text{Li}$ undergoes Bose-Einstein condensation (BEC) [1], the paradigm of all quantum statistical phase transitions. Although fermions cannot directly Bose condense, it is well known that fermions can undergo a BEC-like phase transition in which particles form Cooper pairs \cong . This effect is responsible for electronic superconductivity and for superfluidity of ${}^3\text{He}$.

In this paper, we describe our experiments with ultracold lithium atoms. These experiments include the first direct observation of the growth and collapse of a condensate with attractive interactions, molecular spectroscopy of a Bose-Einstein condensate, and progress towards observing Cooper pairing of ${}^6\text{Li}$ atoms.

Molecular Spectroscopy of a Bose-Einstein Condensate

The ability to cool and trap atoms has enabled many new discoveries in many-body physics and in low-energy collision physics over the past few years. The same capabilities have not, however, been extended to molecules despite strong motivations to do so. Ultracold trapped molecules might, for example, lead to the extension of Bose-Einstein condensation to larger and more complex systems, or to the ability to coherently control chemical reactions. As with atoms, much greater understanding of interparticle interactions, both atom-molecule and molecule-molecule, could be gained through spectroscopic studies involving ultracold molecules.

One way to produce ultracold trapped molecules is to photoassociate ultracold trapped atoms. Fig. 1 shows a schematic diagram for the case of ^7Li . The frequency difference $\omega_2 - \omega_1$ between two lasers is tuned to the binding energy, E_B , of a vibrational level of the ground-state of the diatomic molecule. We performed a similar experiment several years ago in a 1 mK gas of lithium atoms confined to a magneto-optical trap (MOT) [2]. The goal of that experiment was to precisely measure E_B of the least-bound vibrational level ($v=10$) so that the s -wave scattering length of lithium could be accurately determined. In the current experiment, the gas is much colder, ~ 100 nK, and it has undergone Bose-Einstein condensation. Furthermore, since the new

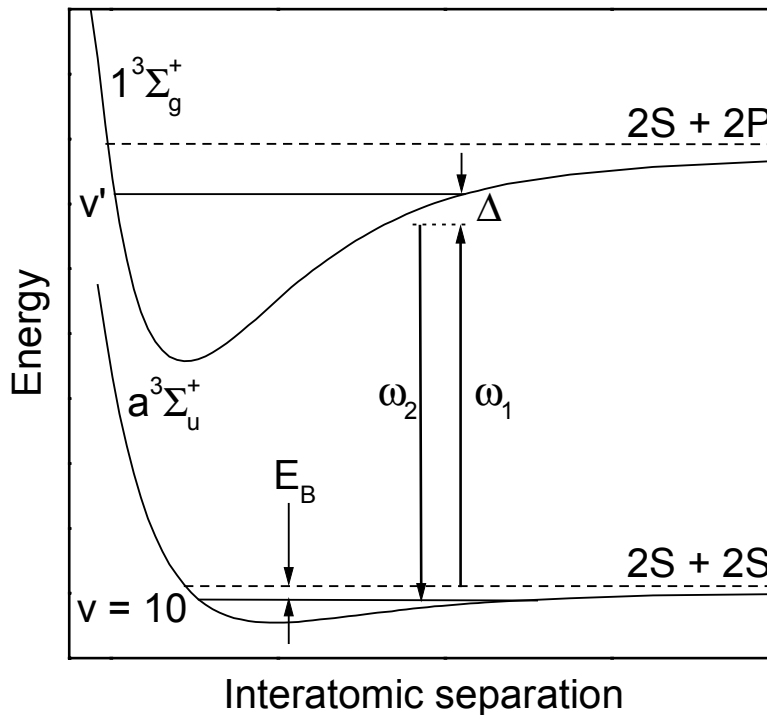


Figure 1: Schematic diagram of two-photon photoassociation.

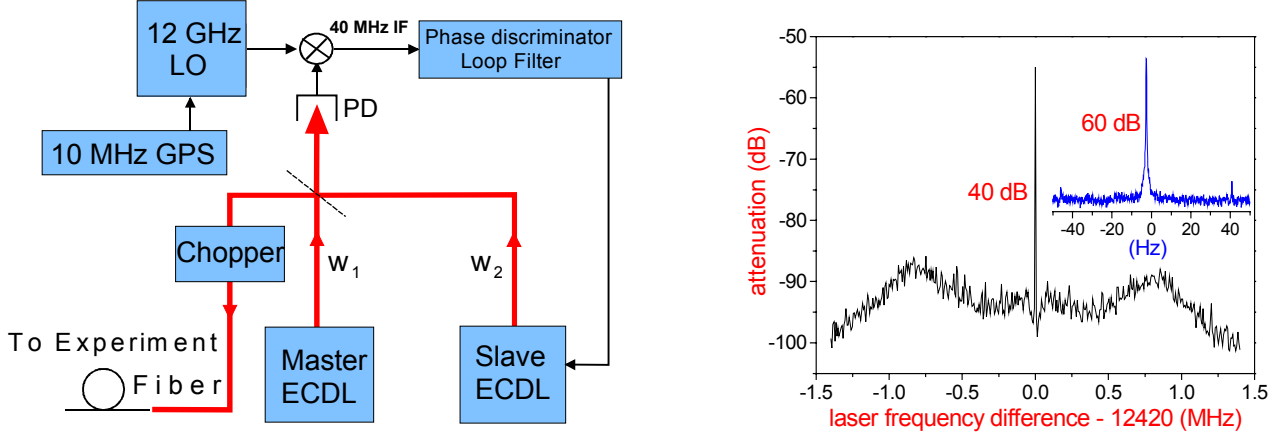


Figure 2: Phase-locked laser system.

experiment is performed in a magnetic trap using spin-polarized atoms, any molecules that are produced will have magnetic moments, and therefore, may be trapped. A similar experiment was recently performed using a Bose-Einstein condensate of rubidium atoms, and the effect of atom-molecule interactions was observed [3].

Since the atoms are extremely cold and the molecules may be relatively long-lived, the two-photon transition linewidth is potentially very narrow. In order to realize this potential sensitivity, two extended-cavity diode laser systems were phase-locked, as shown in Fig. 2. The resulting relative linewidth is under 1 Hz.

The apparatus used to produce BEC of ${}^7\text{Li}$ has been described previously [4]. Permanent magnets establish an Ioffe-Pritchard type trap with an energy depth of 10 mK, a bias field of 1004 G at the trap center, and a nearly spherically symmetric, harmonic trapping potential with an average oscillation frequency of $(\omega_x \omega_y \omega_z)^{1/3} = 2\pi \times 144.5$ Hz. Approximately 2.5×10^8 atoms in the $F = 2$, $m_F = 2$ hyperfine sublevel of ${}^7\text{Li}$ are directly loaded into the trap from a laser-slowed atomic beam. Following loading, the atoms are evaporatively cooled to quantum degeneracy using a microwave field to selectively spin-flip and remove the hottest atoms. Destructive phase-contrast imaging is used to determine the total number of atoms N , their temperature T , and N_0 [4].

Fig. 3 shows a spectrum when $N \approx 10^6$ and $T \approx 700$ nK. Because ${}^7\text{Li}$ has attractive interactions, however, N_0 is always less than ~ 1250 atoms [5]. The signal shown in Fig. 3 is the number of remaining atoms following a pulse of the photoassociating light. The spectrum is distinctly asymmetric. The high-energy side of the line is broadened by the thermal energy distribution, $e^{-E/kT}$, while the low-energy side is very sharp, having a linewidth of less than 3 kHz.

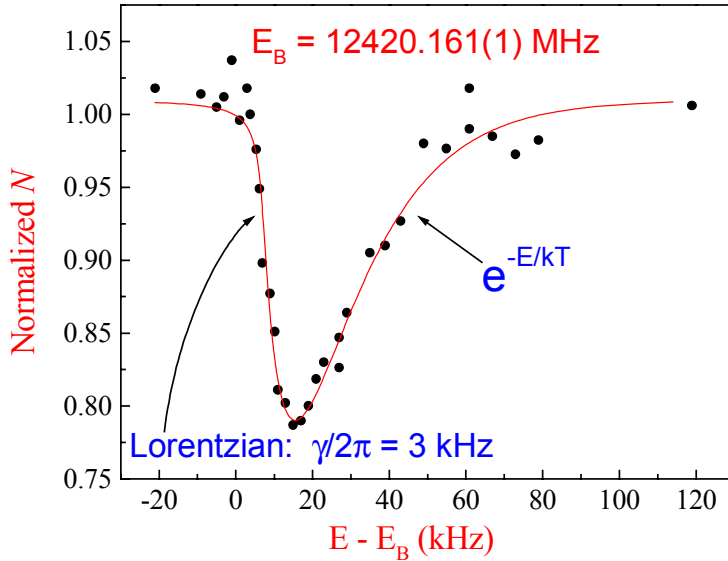


Figure 3: Two-photon photoassociation signal. Signal is number of remaining atoms.

Fig. 4 shows another spectrum, but in this case, the signal is the number of remaining *condensate* atoms rather than the remaining total number. Under these conditions, the entire energy distribution is measured, including the condensate itself. The condensate peak is extremely narrow, its width being ~ 250 Hz. There are several possible sources of broadening. The laser beam of frequency ω_2 (Fig. 1) can induce a transition from the ground-state vibrational level, $v=10$, to the vibrational level v' of the electronically excited state which serves as the intermediate state for the two-photon transition. Although the lasers are detuned by ~ 100 MHz from this intermediate state, off-resonant excitation is possible, and spontaneous emission can occur. A second source of broadening arises from the mean-field interaction between the molecules and the inhomogeneously distributed atomic condensate. And finally, the $v=10$ level itself may be unstable due to vibrational relaxation collisions between molecules and atoms. This process has never been measured, and theoretical estimates are extremely difficult and are available only for collisions between H_2 and H [6]. From the observed width of the condensate feature, we obtain an upper limit of $2 \times 10^{-10} \text{ cm}^3 \text{ s}^{-1}$ for the rate constant for vibrational relaxation collisions between Li_2 ($v=10$) and Li atoms.

Growth and Collapse of a Bose-Einstein Condensate

Interactions between ^7Li atoms are effectively attractive. The dynamical behavior of Bose-Einstein condensation in a gas with attractive interactions is quite striking. Quantum theory predicts that Bose-Einstein condensation (BEC) of a spatially homogeneous gas with

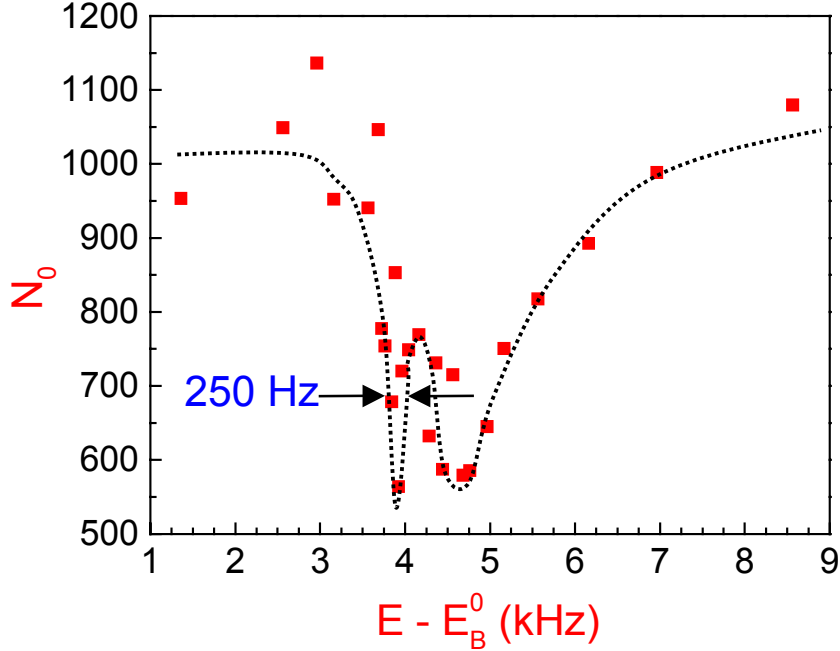


Figure 4: Signal is number of remaining condensate atoms. The peak at low-energies is from the condensate.

attractive interactions is precluded by a conventional phase transition into either a liquid or solid [7]. However, we have demonstrated that when confined to a trap, such a condensate can form [1], provided that the condensate occupation number does not exceed a limiting value [5,8]. When the stability limit is exceeded, the repulsive force arising from position-momentum uncertainty under conditions of spatial confinement, is overcome by self-attraction, causing the condensate to collapse [9-13].

Condensate growth is initiated by cooling a gas below the critical temperature T_c for BEC. For attractive interactions, N_0 grows until the maximum number is reached, at which point the condensate collapses. The collapsing condensate can be compared to a star going supernova: during the collapse, the density rises giving a sharp increase in the rate for collisions, both elastic and inelastic. These collisions cause atoms to be ejected from the condensate in an energetic explosion. Condensate growth, fed by collisions between thermal atoms in the gas, will continue until the gas reaches thermal equilibrium, resulting in a series of sawtooth-like cycles of condensate growth and collapse [13]. We previously attained evidence for this nonequilibrium dynamical behavior by measuring the distribution of N_0 at selected times following a fast quench of a gas of ^7Li atoms [14]. N_0 was found to be distributed between small numbers, $N_0 \approx 100$, and the maximum number of ~ 1250 atoms, in agreement with the growth and collapse model.

Accurate measurements of small values of N_0 necessarily destroy the condensate, and it has not been possible, therefore, to observe the condensate dynamics in real time. However, we have now directly observed the initial growth and collapse of a Bose-Einstein condensate by using the two-photon transition to deplete the condensate. Because of the high spectral resolution of the two-photon transition, the thermal atoms are only minimally affected. This process synchronizes the growth and collapse cycles for different experiments at a particular point in time, which enables the growth/collapse dynamics to be observed by simply repeating the experiment, and measuring N_0 at different delays following the two-photon pulse.

In order to stimulate rapid growth and collapse conditions, a 100 ms duration microwave quench pulse is applied following evaporative cooling. This pulse removes $\sim 80\%$ of the atoms, leaving all but the coldest $\sim 10^5$ atoms. This quench pulse leaves the gas far from thermal equilibrium, and if left to freely evolve, the condensate will alternately grow and collapse many times for a period of ~ 30 s [14]. After a delay of either 3 or 5 s following the microwave quench pulse, a light pulse consisting of two co-propagating laser beams tuned to the two-photon transition dumps the condensate. Once in the molecular state, the laser of frequency ω_2 can stimulate a single-photon transition to the intermediate level v' (Fig. 1), which can then spontaneously decay into a state of two energetic atoms that escape the trap. This method for removing atoms is very energy specific since the observed two-photon linewidth of 250 Hz is much less than the ~ 5 kHz thermal energy spread of the trapped atoms. In particular, the condensate may be selectively removed without significantly affecting the remaining atoms.

Following the light pulse, the gas is allowed to freely evolve for a certain time, at which point a destructive measurement of N_0 is made. Figure 5a shows the dynamical evolution of the condensate following a light pulse whose duration is adjusted to reduce N_0 to an initial value ~ 100 atoms. Each data point corresponds to a given delay following the light pulse, and is the mean of five separate measurements of N_0 . The error bars are the uncertainty in the mean. The statistical uncertainty in N_0 is ± 65 atoms, while the systematic uncertainty, dominated by uncertainties in the imaging system, is $\pm 20\%$ [14]. Immediately following the light pulse, N_0 increases, as the condensate is fed via collisions between noncondensed thermal atoms, and N_0 reaches a maximum value consistent with the expected upper limit of 1250 atoms. A collapse is clearly indicated by the subsequent reduction in N_0 . After the collapse, N_0 grows again, since the gas is not yet in thermal equilibrium. We verified that additional peaks are observed when the initial growth rate is increased by removing fewer atoms from the condensate. For the data shown in Fig. 5b, N_0 is set to an initial value of ~ 400 atoms, and two secondary peaks are clearly discernable. In Fig. 5c, N_0 is set to very small numbers, which, as discussed below, causes the rate of growth to slow. These measurements represent the first direct observation of growth and

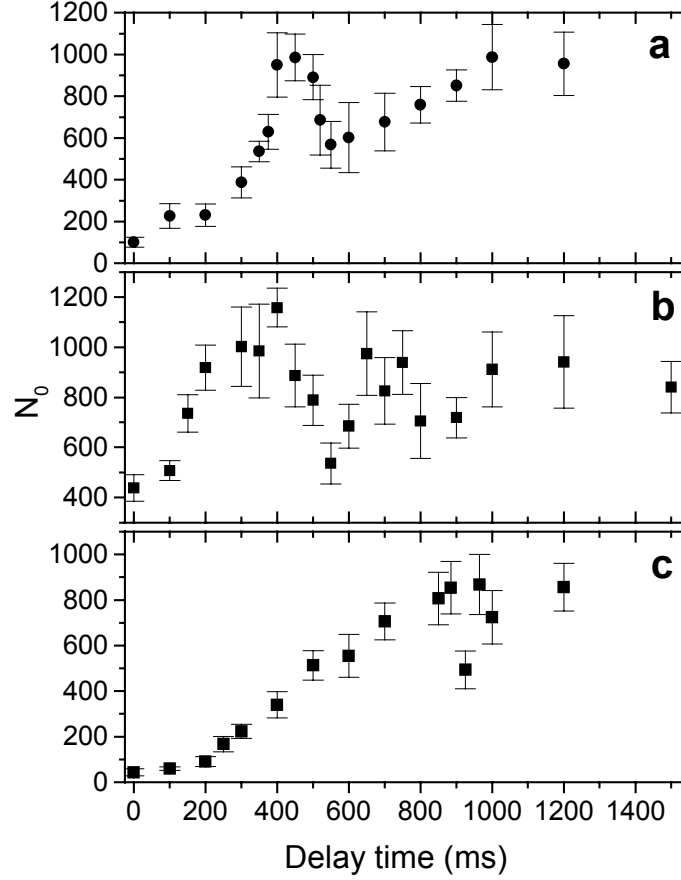


Figure 5: Condensate growth and collapse.

collapse dynamics.

The data represent an average of many trajectories whose initial phase and rate of growth differ slightly. To analyze the results, we numerically simulated the collisional redistribution of atoms over the energy states of the trap using the quantum Boltzmann equation, as described in detail in ref. [13]. The colored curves shown in Fig. 6 are a sample of simulated trajectories which include the effect of the microwave quench pulse and the light pulse. The variation in condensate growth following a dump pulse is mainly the result of slight differences in the initial number of atoms loaded into the trap. A different initial number leads to variations in energy distribution following evaporative cooling, which in turns contributes to variation in the condensate growth rate. Additionally, the stochastic nature of the collapse process, which causes each collapse to occur at a slightly different value of N_0 , also contributes to the variation in condensate growth. The heavy black line represents the average of 20 curves obtained by choosing the initial number within a 10% range. The experimental results are remarkably well-described by this simulation. Other parameters, such as the initial number and temperature of the

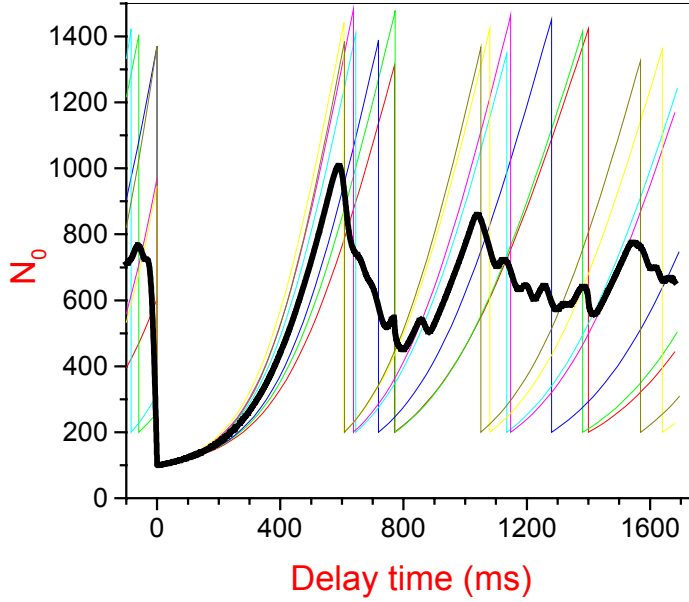


Figure 6: Simulation of condensate dynamics.

atoms, and those associated with the spectral location and power-broadened width of the two-photon dump pulse, were taken from the actual experimental data. In the simulations, N_0 is set to 200 atoms immediately following a collapse in agreement with our previous result [14].

BCS Phase Transition of ${}^6\text{Li}$

An exciting new direction in the ultra-cold atom field is to produce a quantum degenerate Fermi gas. Under a grant from the NASA Microgravity Research Division, we have begun an experiment to produce an ultra-cold gas of ${}^6\text{Li}$ atoms. As with the Bose gases, much of the interesting physics has to do with the interactions between atoms. ${}^6\text{Li}$ is particularly intriguing because, by a fluke of nature, the interactions between two atoms is enormously large and attractive [15], enabling perhaps, the first observation of a Bardeen-Cooper-Schrieffer (BCS) phase transition to a superfluid state of a gas [16].

The BCS theory was developed to explain superconductivity and has also been applied to superfluid ${}^3\text{He}$. The fundamental effect underlying these phenomena is the pairing of particles, known as Cooper pairing. In 1980, Leggett considered whether such a transition could be observed in deuterium [17]. He showed that the transition temperature $T_c \approx (5 E_F / 3 k_B) \exp[-\pi / (2 k_F |a|) - 1]$, where k_F is the Fermi wave number and a is the s -wave scattering length. In deuterium $a \approx -7 a_0$, and Leggett concluded that T_c is too low for there to be any hope of seeing

the transition in the gas phase. However, Stoof *et al.* recently pointed out that ${}^6\text{Li}$ is the ideal candidate for such an experiment, given that a is over 300 times larger than for deuterium [16]. With 200,000 atoms, a number of atoms with which we are able to produce degenerate gases of ${}^7\text{Li}$, the simple expression above gives an experimentally accessible $T_c \approx 25$ nK.

The apparatus and techniques we will use to produce a degenerate gas of ${}^6\text{Li}$ are similar to those used for ${}^7\text{Li}$ [1,5]. Atoms are loaded into a magnetic trap from an atomic beam source, they are laser cooled to ~ 200 μK , and then evaporatively cooled to the nK regime. The primary difference between the Boson experiments and the Fermion experiment arises because of the Pauli Exclusion Principle, which forbids identical Fermions interacting via a s -wave. This fact complicates the usual evaporative cooling technique used so successfully with Bose gases, because of the inability of identical Fermions to undergo the necessary thermalization collisions. We plan to circumvent this difficulty by cooling the ${}^6\text{Li}$ atoms Asympathetically \equiv [18,19] via their interactions with evaporatively cooled ${}^7\text{Li}$ atoms. This adds complexity to the experiment because both isotopes must be simultaneously trapped.

We have successfully loaded both ${}^6\text{Li}$ and ${}^7\text{Li}$ atoms into a new magnetic trap apparatus. In both cases, we begin by loading a magneto-optical trap (MOT). In the case of ${}^7\text{Li}$, atoms are loaded into the MOT by laser slowing a thermal atomic beam using the Zeeman slower technique. Approximately 10^{10} ${}^7\text{Li}$ atoms are loaded into the MOT at a temperature of 500 μK . Of these, $\sim 10\%$ are transferred to the magnetic trap, and over 10^6 have been evaporatively cooled to temperatures below 1 μK (see Fig. 7). The ${}^6\text{Li}$ atoms are loaded using a newly-developed laser-free technique that we have named the Askimmer \equiv [20]. For ${}^6\text{Li}$, 3×10^8 atoms have been loaded into the MOT and $\sim 5 \times 10^7$ atoms have been transferred to the magnetic trap. Since this is a sufficient number of ${}^6\text{Li}$ atoms, the next step will be to evaporatively cool the ${}^7\text{Li}$ atoms in the presence of ${}^6\text{Li}$. We hope to have at least 10^6 atoms in the degenerate regime.

There are several possible manifestations of the BCS phase-transition that we will look to as signatures, but there is opportunity for much more theoretical work to fully understand the implications. Perhaps the best possibility is to optically image the Fourier transform of the density distribution of the gas, which should be sensitive to the momentum pair-distribution function of the trapped atoms [21]. Calculations show that the length scale of the pair correlation function is much smaller than the size of the trapped atom cloud. Therefore, the presence of pairs should result in large angle scattering that could be detected using the usual imaging techniques

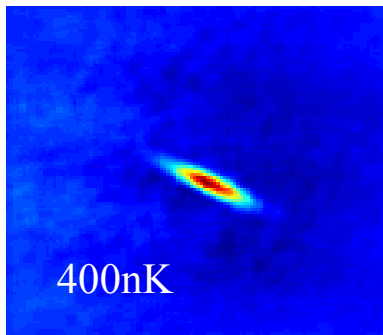
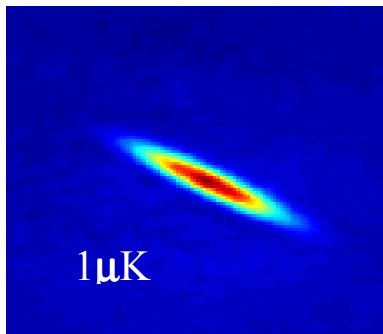
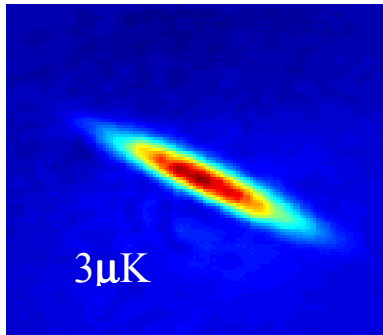
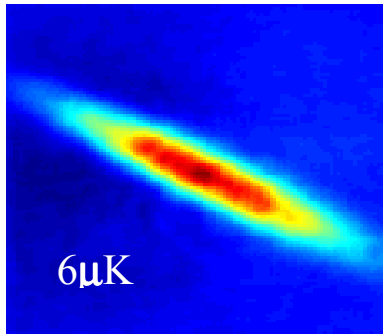


Figure 7: Evaporative cooling of ${}^7\text{Li}$.

developed to image Bose-Einstein condensates of trapped atoms.

Conclusions and Outlook

The opportunity to study degenerate gases is very exciting. ${}^6\text{Li}$ is particularly interesting because it is a Fermion with an enormously large attractive interaction, which may provide the means to observe a BCS phase transition to a gaseous superfluid state. Microgravity environments may be very important in ultra-cold atom experiments due to the simple fact that the gravitational potential is comparable to, or even larger than the kinetic temperature of the atoms. The effect of gravitational forces on evaporative cooling must already be considered in ground-based experiments, and may be expected to effect delicate phase transitions, such as the BCS transition of ${}^6\text{Li}$.

The authors wish to thank the NASA Microgravity Research Division for their support of this program.

References

1. C. C. Bradley, C. A. Sackett, J. J. Tollett, and R. G. Hulet, Phys. Rev. Lett. **75**, 1687 (1995).
2. E. R. I. Abraham, W. I. McAlexander, C. A. Sackett, and R. G. Hulet, Phys. Rev. Lett. **74**, 1315 (1995).
3. R. Wynar, R. S. Freeland, D. J. Han, C. Ryu, and D. J. Heinzen, Science **287**, 1016 (2000).
4. C. A. Sackett, C. C. Bradley, M. Welling, and R. G. Hulet, Applied Physics B **65**, 433 (1997).
5. C. C. Bradley, C. A. Sackett, and R. G. Hulet, Phys. Rev. Lett. **78**, 985 (1997).
6. R. C. Forrey, V. Kharchenko, N. Balakrishnan, and A. Dalgarno, Phys. Rev. A **59**, 2146 (1999).
7. N. Bogolubov, J. of Phys. **XI**, 23 (1947); H. T. C. Stoof, Phys. Rev. A **49**, 3824 (1994).
8. P. A. Ruprecht, M. J. Holland, K. Burnett, and M. Edwards, Phys. Rev. A **51**, 4704 (1995).
9. Y. Kagan, G. V. Shlyapnikov, and J. T. M. Walraven, Phys. Rev. Lett. **76**, 2670 (1996).

10. E. Shuryak, Phys. Rev. A **54**, 3151 (1996).
11. H. T. C. Stoof, J. Stat. Phys. **87**, 1353 (1997).
12. M. Ueda and A. J. Leggett, Phys. Rev. Lett. **80**, 1576 (1998).
13. C. A. Sackett, H. T. C. Stoof, and R. G. Hulet, Phys. Rev. Lett. **80**, 2031 (1998).
14. C. A. Sackett, J. M. Gerton, M. Welling, and R. G. Hulet, Phys. Rev. Lett. **82**, 876 (1999).
15. E. R. I. Abraham, W. I. McAlexander, J. M. Gerton, R. G. Hulet, R. Côté, and A. Dalgarno, Phys. Rev. A **55**, R3299 (1997).
16. H. T. C. Stoof, M. Houbiers, C. A. Sackett, and R. G. Hulet, Phys. Rev. Lett. **76**, 10 (1996); M. Houbiers, R. Ferwerda, H. T. C. Stoof, W. I. McAlexander, C. A. Sackett, and R. G. Hulet, Phys. Rev. A **56**, 4864 (1997).
17. A. J. Leggett, J. Phys. (France) IV **C7**, 19 (1980).
18. D. J. Larson, J. C. Bergquist, J. J. Bollinger, W. M. Itano, and D. J. Wineland, Phys. Rev. A **57**, 70 (1986).
19. C. J. Myatt, E. A. Burt, R. W. Ghrist, E. A. Cornell, C. E. Wieman, Phys. Rev. Lett. **78**, 586 (1997).
20. B. Ghaffari, J. M. Gerton, W. I. McAlexander, K. E. Strecker, D. M. Homan, and R. G. Hulet, Phys. Rev. A **60**, 3878 (1999).
21. Weiping Zhang, C. A. Sackett, and R. G. Hulet, Phys. Rev. A **60**, 3878 (1999).

PROGRESS ON PARCS

T.P. Heavner, L.W. Hollberg, S.R. Jefferts, D.M. Meekhof, T.E. Parker, W.D. Phillips,
S.L. Rolston, H.G. Robinson, J.H. Shirley, D.B. Sullivan, F.L. Walls
National Institute of Standards and Technology - U.S.A.
N. Ashby - University of Colorado - U.S.A.
W.M. Klipstein, L. Maleki, D.J. Seidel, R.J. Thompson, S. Wu, and L. Young
Jet Propulsion Laboratory - U.S.A.
R.F.C. Vessot E.M. Mattison - Harvard Smithsonian Center for Astrophysics - U.S.A.
A. DeMarchi - Politecnico di Torino - Italy

This paper describes progress toward development of a Primary Atomic Reference Clock in Space (PARCS) and reviews scientific and technical objectives of the PARCS mission. PARCS is a collaborative effort involving the National Institute of Standards and Technology, the University of Colorado, the Jet Propulsion Laboratory, the Harvard Smithsonian Center for Astrophysics and Politecnico di Torino. The experiment involves a laser-cooled cesium atomic clock, a Global Positioning System (GPS) time-transfer system, and a hydrogen maser that serves as both a local oscillator for the cesium clock and a reference against which tests of gravitational theory can be made.

1. Introduction

In the microgravity environment of the International Space Station (ISS), cesium atoms can be launched more slowly through the clock's microwave cavity, reducing a number of effects (including systematic effects), thus improving the performance of an atomic clock well beyond that achieved on earth. A more accurate and stable clock in space can be used for several purposes including: tests of gravitational theory, study of GPS satellite clocks, study of neutral atoms in microgravity, and more-accurate realization of the second, which can then be made available worldwide. PARCS¹ and two other cooled-atom-clock programs, Atomic Clock Ensemble in Space (ACES)² and Rubidium Atomic Clock Experiment (RACE)³ are also scheduled for flight on the International Space Station (ISS).

Several relativistic effects on clocks will be measured in this experiment. Significant measurements include the gravitational frequency shift, which can be determined nearly two orders of magnitude more accurately than was done previously, and local position invariance, which can be tested more than three orders of magnitude more accurately than the best current experiments on earth. Should this experiment fly concurrently with SUMO (Superconducting Microwave Oscillator)⁴, which is also scheduled to fly on the ISS, local position invariance can be tested more than four orders of magnitude better than current experiments and a Kennedy-Thorndike test can be done five orders of magnitude better than the most accurate experiments done on earth. Finally, the realization of the second in space can be achieved at an uncertainty of 5×10^{-17} , a factor of 20 better than that achieved on earth.

PARCS completed its Science Concept Review in January 1999 and is scheduled for a Requirements Design Review in the Fall of 2000. Preliminary designs of many components are nearing completion and a number of prototype components have been developed and are being tested. PARCS is currently scheduled to fly in late 2004 to early

2005. The rest of this paper closely follows the material presented at this workshop (Fundamental Physics in Microgravity Workshop, Solvang, CA, 19-21 June, 2000).

2. System Design

As shown in Figure 1, the experiment is projected to be located on a forward section of the Japanese Experimental Module (JEM) External Facility (EF). This location provides reasonable zenith and nadir views, which are important for time transfer. Furthermore, the available power (3 kW), closed-fluid cooling (2 kW), and space ($1.8 \times 1.0 \times 0.8$ m) are well suited to the experiment requirements.

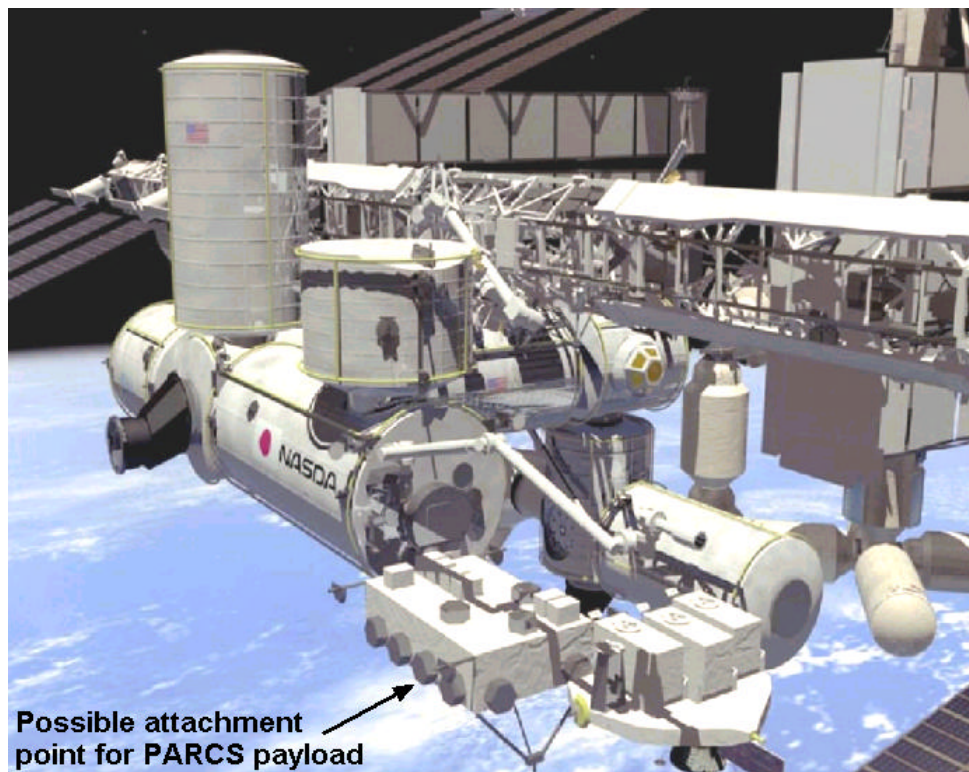


Figure 1. Projected location of PARCS on the ISS.

Figure 2 shows a block diagram of the main space and earth components. The local oscillator is a space-qualified hydrogen maser produced (but never flown) for MIR. The output of the maser is fed to the low-phase-noise microwave synthesizer, which, under control of the computer, produces frequency offsets steered to the appropriate locations on the cesium spectrum. The synthesizer also delivers a reference signal at the cesium resonance frequency to the GPS receiver for common-view comparisons with atomic clocks on earth. The GPS common-view method is described below. Clock control signals, as well as clock and GPS-receiver data, are sent through the relatively low-data-rate communication link shown at the top right of Fig. 2.

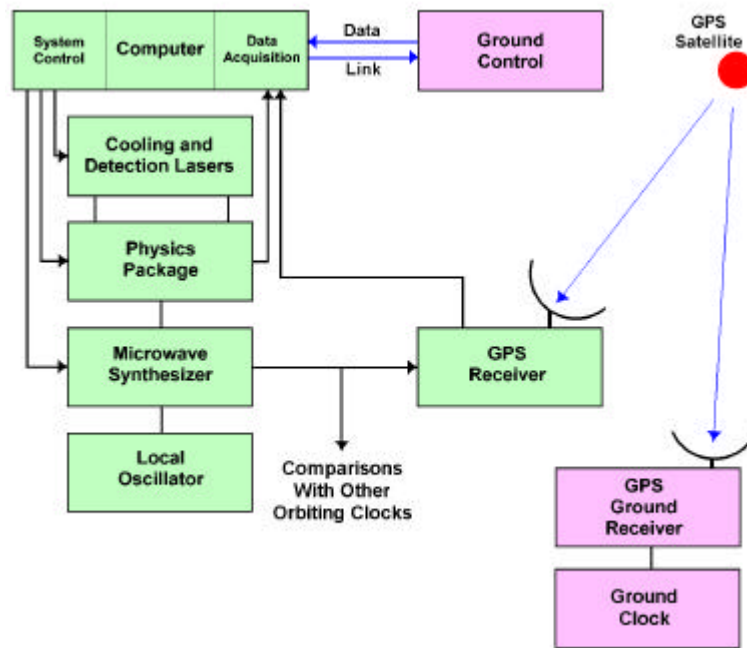


Figure 2. Block diagram of the PARCS experiment showing the major ISS and ground-station components.

Transfer of time and frequency are accomplished using reception of the GPS carrier (phase) in a common-view method shown schematically in Figure 3. Receivers at point A (an earth ground station) and point B (on the ISS) receive the same signal from one individual GPS satellite. The data acquired at each location is the difference between the reference clock at that location and the GPS clock, with an added signal-transit delay. In differencing the data sets acquired at the two points, the GPS clock drops out, and we are left with the difference, $A - B$, between the two clock readings, plus the differential transit delay. The delay term has some common-mode components. Using ionospheric-delay data obtained from dual-frequency GPS measurements and tropospheric delay estimates, the difference term can be evaluated quite well. Dramatic improvement over single observations is then obtained by taking and averaging additional clock differences using all available GPS satellites within common view of the two observing stations. The best result for measurements of this type (for two earth stations) has been an RMS time noise of 30 ps.

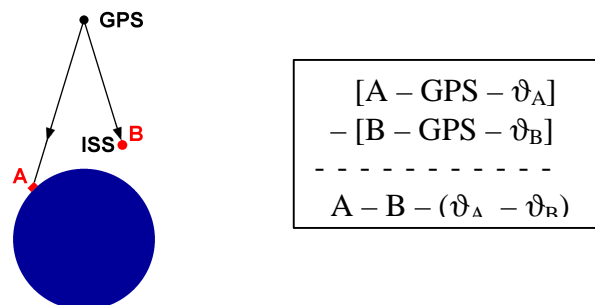


Figure 3. GPS common-view method. Signals received at A and B produce the clock differences shown in the first two lines, and the difference between these data removes the GPS reference time as shown.

Figure 4 shows the limitations imposed by time transfer with both 10 ps and 50 ps stability. For the time-transfer-system limits alone, the two curves would continue downward, but measurements are ultimately limited by uncertainties in the position of the ISS. The flattening of the time-transfer curves represents a positional uncertainty of 10 cm. The stability of the cesium clock is shown as the straight line below the time transfer curves. The averaging times required to reach particular points on the curve are shown. Figure 4 shows that the time transfer system is clearly going to limit comparisons between the PARCS clock and clocks on the earth. At the selected stability of $s_y(t) = 5 \times 10^{-14}$, time transfer is the limiting factor.

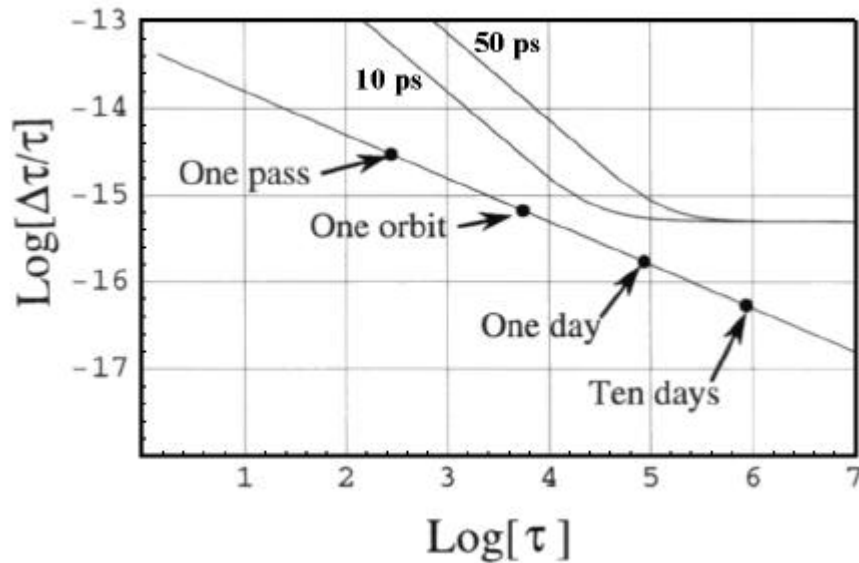


Figure 4. Stability as a function of averaging time t for both the time-transfer system and the PARCS clock. Some specific averaging times are shown on the clock stability. The flattening of the time-transfer curves results from uncertainty in the location of the ISS.

The space-clock concept is shown in Fig. 5. Atoms are cooled, collected, and launched in the atom-preparation region. The clock arrangement is similar to a conventional atomic-beam clock on earth, except that the atoms are cooled and launched as a sequence of balls that proceed through the Ramsey (microwave) cavity to the state-detection region. Shutters at both the launch and detection ends are closed during any laser interaction with the atoms. This prevents scattering of laser light into the cavity region where this near-resonant light would otherwise significantly shift the frequency.

The atoms are cooled and trapped using conventional optical-molasses techniques. For frequency measurements on each side of the resonance, a large number of atom balls are launched and detected before the frequency is moved to the other side of the line. This minimizes the stability limit produced by the dead time (the Dick effect). To achieve the desired stability, we estimate that we must launch 2 balls per second with a transverse temperature of $2 \mu\text{K}$ and 1.1×10^7 atoms in each ball at a velocity of 15

cm/s. For a cavity length of 75 cm, this gives a Ramsey time of 5 s. The cycle time (the time spent in frequency measurement on each side of the line) is projected to be 20 s. These parameters are within the state of the art, and a trap system was constructed to verify that we could achieve them.

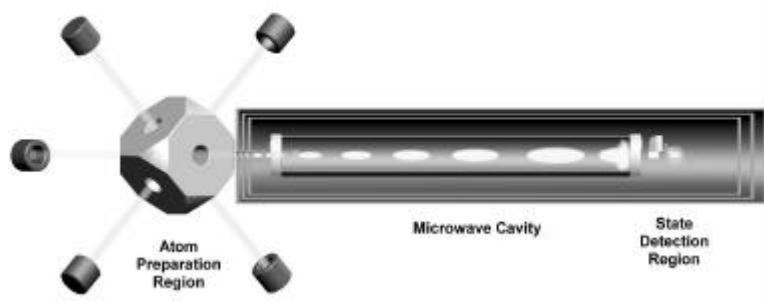


Figure 5. Diagram of the PARCS laser-cooled space clock. Atoms in the source (atom-preparation) region are cooled and trapped and then launched. The state-detection lasers are not shown. State detection involves, not only detection of the atoms that have changed states, but also measurement of the number of atoms arriving in each measurement cycle so as to normalize detection to the number of atoms launched and thus remove shot-to-shot noise. Shutters (not shown) at ends of the cavity are closed during laser interactions with atoms to prevent scattering of laser light into the cavity. Three concentric magnetic shields are shown surrounding the microwave cavity and state-detection region.

Figure 6 is a simple sketch of the layout of the clock with dimensions roughly to scale. The cavity outline is the outside of the cavity. The lower portion of the figure shows the system dimensions in greater detail.

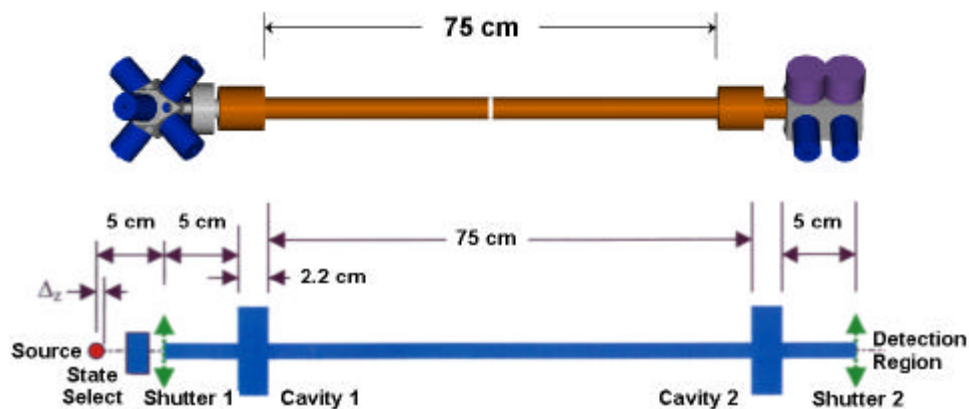


Figure 6. Dimensions for the PARCS clock.

One of the larger systematic frequency shifts to be evaluated and corrected is the spin-exchange frequency shift. This shift is large (0.5 to 1×10^{-15}) for typical earth-bound clocks). Fortunately, this shift scales down dramatically with increasing Ramsey time and is projected to be nearly two orders of magnitude smaller for the chosen PARCS parameters. The spin-exchange and other systematic shifts will have to be carefully measured and corrected to achieve the desired long-term stability, but there appear to be no major issues associated with correcting these shifts.

It has long been recognized that the spin-exchange shift in rubidium is much smaller than that in cesium, and therefore it might be a good candidate for advanced atomic clocks. While this is true, the spin-exchange shift is not a limiting consideration for PARCS. There are several advantages to staying with cesium, including the facts that (1) the cavity can be smaller (because the resonance frequency is higher) and that (2) the definition of the second is based on cesium. This will allow PARCS to serve as a primary standard for the world.

3. Prototype Development

A number of components have been either designed or fabricated in prototype form. These include the following.

- The shutters, which are critical to operation of the PARCS clock, have recently been fabricated, and preliminary testing of them has begun. These shutters must produce a minimum of magnetic field and vibration, have an open aperture of 1.0 cm, operate at a rate of at least 10 Hz, and survive $\sim 2 \times 10^8$ actuations.
- Collimators for the trapping and detection lasers, as well as a prototype trapping chamber, have been constructed from titanium, and a prototype for the clock will be assembled over the next few months.
- A microwave synthesizer with a performance well beyond that needed for PARCS has been constructed, and measurements of phase stability confirm that it meets the required performance. A second synthesizer, incorporating features that better match it to PARCS, and that uses a number of space-qualified components, is nearing completion.
- Preliminary designs for the laser system have been produced using, as much as possible, commercially available components. Some components have already been evaluated for vibration immunity. A laser-welding system will be used to assemble a number of the components requiring exacting alignment. A jig system for achieving correct alignment before welding has been constructed.
- A design for the microwave cavity is now complete, and fabrication of the cavity will begin soon.

4. Summary

In summary, PARCS development is proceeding on schedule, and all critical issues are being addressed through modeling and prototype construction. It appears that, as long as shutter problems can be solved, the requirements for atom density and systematic frequency shifts should be achievable.

5. References

- * Contribution of the U.S. Government, not subject to copyright.
- 1. S.R. Jefferts, T.P. Heavner, L.W. Hollberg, J. Kitching, D.M. Meekhof, T.E. Parker, W. Phillips, S. Rolston, H.G. Robinson, J.H. Shirley, D.B. Sullivan, F.L. Walls, N. Ashby, W.M. Klipstein, L. Maleki, D. Seidel, R. Thompson, S. Wu, L. Young, and A. DeMarchi, "PARCS: a primary atomic reference clock in space," *Proc. 1999 Joint Meeting of the European Frequency And Time Forum and the IEEE Frequency Control Symposium*, IEEE Cat. No. 99CH36313, pp. 141-144 (1999).
- 2. S. Feltham, F. Gonzalez, and P. Puech, "ACES: a time and frequency mission for the international space station," *Proc. 1999 Joint Meeting of the European Frequency And Time Forum and the IEEE Frequency Control Symposium*, IEEE Cat. No. 99CH36313, pp. 148-151 (1999).
- 3. C. Fertig, K. Gibble, B. Klipstein, J. Kohel, L. Maleki, D. Seidel, and R. Thompson, "Laser-cooled microgravity clocks," *Proc. 1999 Joint Meeting of the European Frequency And Time Forum and the IEEE Frequency Control Symposium*, IEEE Cat. No. 99CH36313, pp. 145-147 (1999).
- 4. J. Lipa, M. Dong, S. Wang, S. Buchman and J. Turneare, "Status of the superconducting microwave oscillator clock experiment," *Proc. 1998 NASA/JPL Microgravity Fundamental Physics Workshop*, June 23-25, 1998, Oxnard, CA, NASA Document D-18442, pp. 309-316 (1999).

CANCELLATION OF THE ^{87}Rb COLD COLLISION SHIFT AND THE RACE DESIGN

Chad Fertig, Jérémie Bouttier, and Kurt Gibble

Yale University, New Haven, CT 06511

Bill Klipstein, Lute Maleki, David Seidel, and Rob Thompson

Jet Propulsion Laboratory, Pasadena, CA 91109

ABSTRACT

We demonstrate a prototype of a laser-cooled ^{87}Rb fountain clock and measure the frequency shift due to cold collisions. The shift is fractionally 30 times smaller than that in a laser-cooled Cs clock. We observe a density dependent pulling by the microwave cavity and use it to cancel the collision shift. We have also demonstrated a juggling atomic fountain to study cold collisions and we discuss the importance of juggling for future fountain clocks.

The design for RACE, a Rb clock flight experiment for the ISS, is described. The cold collision shift and multiple launching (juggling) have important implications for the design and the resulting clock accuracy and stability. We present and discuss the double clock design for RACE. This design reduces the noise contributions of the local oscillator and simplifies and enhances an accuracy evaluation of the clock.

1. INTRODUCTION

The most serious systematic error in laser-cooled clocks is the frequency shift due to cold collisions.¹ Tiesinga *et al.* first calculated this shift² and Gibble and Chu³ measured the shift for laser-cooled Cs clocks to be $\delta\nu/\nu = -1.7 \times 10^{-12}$ at a density of 10^9 cm^{-3} . Due to Cs_2 molecular bound states near zero energy, the frequency shift cross section has nearly the maximal value of $\lambda_{\text{dB}}^2/2\pi$ where λ_{dB} is the de Broglie wavelength. This large cross section led us to examine clocks based on other atoms, for which the cold collision shift might be smaller.^{4,5}

We measure the cold collision shift for ^{87}Rb and cancel the shift by detuning the microwave clock cavity. We have also demonstrated a juggling fountain. Juggling fountain clocks will be able to achieve higher stability without requiring large improvements in signal-to-noise (S/N) or the local oscillator. We discuss the optimal juggling rate and pattern that can cancel the frequency shift due to juggling collisions.

The principal advantage of microgravity for atomic clocks is interrogation times longer than 1s. With a 10 s interrogation time, a clock has a 50 mHz linewidth suggesting that accuracies may approach 10^{-17} . However, to achieve greater accuracy within the same averaging time, greater stability is needed.

RACE, the Rubidium Atomic Clock Experiment, is based on Rb to avoid the large cold collision shift of Cs. This may allow simultaneously high short-term stability and accuracy. For RACE, we have 3 primary goals:

- 1) Demonstrate new clock techniques for laser-cooled atoms to enable frequency comparisons with accuracies of 1 part in 10^{17} .
- 2) Significantly improve the classic clock tests of general relativity.
- 3) Distribute accurate time and frequency from the ISS.

We review the design constraints and discuss the double clock design for RACE.

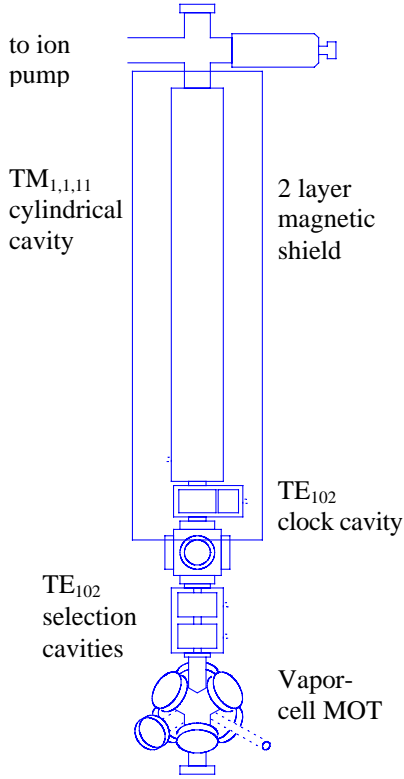


Figure 1. Schematic of ^{87}Rb fountain clock.

2. LASER-COOLED RB CLOCK

A schematic of our ^{87}Rb fountain clock is shown in Fig. 1. Using 0.9W of light from a Ti:Sapphire laser delivered by an optical fiber, atoms are collected from the room temperature Rb vapor in the vapor-cell MOT. The atoms are launched upwards and cooled to $1.8\ \mu\text{K}$ in the moving frame. The atoms then pass through 2 microwave cavities that are normally used to prepare half of the atoms in the $5S_{1/2}\ |F=1, m=0\rangle$ state.⁶ Here, to achieve high density, the selection cavities are not used. Instead, we optically pump the atoms into $|1, -1\rangle$ just below the clock cavity. We use successive pulses of circularly polarized light from diode lasers tuned to the $5S_{1/2}\ F=2 \rightarrow 5P_{3/2}\ F'=1'$ and $1 \rightarrow 1'$ transitions. Microwaves from a horn then transfer atoms from $|1, -1\rangle$ state to the $|2, 0\rangle$ state while a 35 mG horizontal magnetic field is applied along the direction of the optical pumping beams. A vertical magnetic field of 3.5 mG is then applied

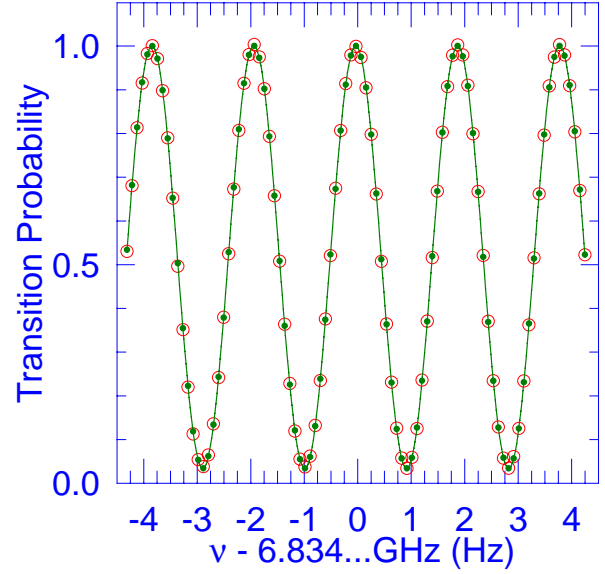


Figure 2. ^{87}Rb Ramsey fringes at 6.834 GHz. The large circles are the data and the small are a fit to the data. The linewidth is 0.95 Hz and the S/N=200.

below the clock cavity as the horizontal bias field is switched off. Microwaves from the horn transfer a variable number of atoms from $|2, 0\rangle$ to $|1, 0\rangle$. Any atoms remaining in $F=2$ are cleared with light tuned to the $2 \rightarrow 3'$ transition. In this way, we can vary the density preparing a maximum of 70% of the atoms in $|1, 0\rangle$ at a temperature of $5\ \mu\text{K}$ with fewer than 1% in $|1, \pm 1\rangle$. To prepare the atoms in $|2, 0\rangle$, we add another microwave pulse to transfer the atoms in $|1, 0\rangle$ to $|2, 0\rangle$ and then repump any atoms in $F=1$ with light tuned to $1 \rightarrow 2'$.

The state prepared atoms enter the magnetic shielding and experience a 6.8 GHz microwave pulse in the rectangular TE_{102} clock cavity, creating a coherent superposition of $|1, 0\rangle$ and $|2, 0\rangle$. This coherence precesses as the atoms are slowed by gravity and return through the clock cavity. The second microwave pulse converts the phase difference between the atomic coherence and the microwave field into a population difference. We detect the transition probability using a laser tuned to $2 \rightarrow 3'$ producing Ramsey fringes as in Fig. 2. To normalize the fringes, we also detect the total number of atoms by repumping the population in $|1, 0\rangle$ using a laser beam tuned $1 \rightarrow 2'$, followed by a second detection

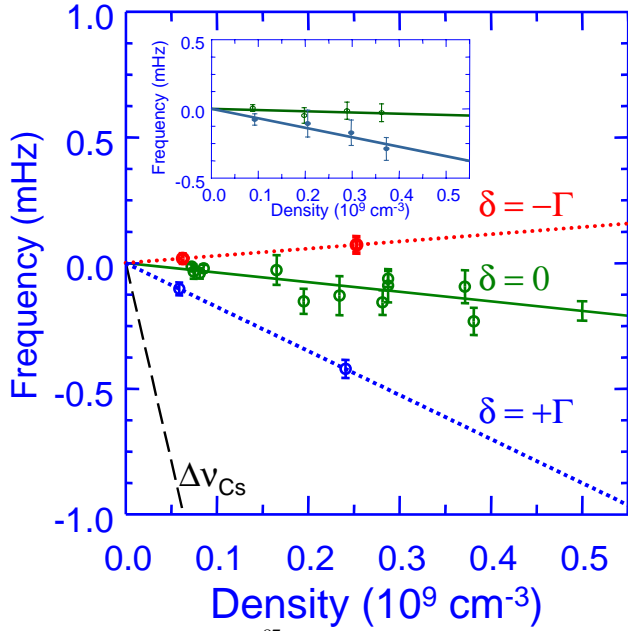


Figure 3. Measured ^{87}Rb cold collision shift (circles and solid line). The shift is $-0.38(8)$ mHz for a density of $1.0(6)\times 10^9$ cm^{-3} . The dashed line is the measured shift for Cs.³ The dotted lines (diamonds and squares) show the density dependence for clock cavity detunings of $\delta = \pm\Gamma$. The inset shows a cancelled collision shift for $\delta = -30$ kHz and atoms prepared in $|1,0\rangle$.

laser pulse. In Fig. 2, the interrogation time is $T=0.526$ s which gives a linewidth of $\Delta\nu=0.950$ Hz. With our detection signal-to-noise $S/N=500$ on a single launch, the atomic transition frequency⁷ of $6,834,682,610.9$ Hz can be determined in 1 s with a precision of $\delta\nu/\nu = \Delta\nu/\pi\nu S/N = 9\times 10^{-14}$. However, the short-term instability of our local oscillator limits the S/N to 200 or $\delta\nu/\nu = 2.1\times 10^{-13}$ for 1s of averaging. The magnetic bias field is 710 μG in the cavity and flight region which we probe by exciting a $\Delta m=1$ (sigma) transition in the cylindrical $\text{TM}_{1,1,11}$ cavity. The fractional quadratic Zeeman shift¹ for this field is $\delta\nu/\nu = 4\times 10^{-14}$.

During the precession time above the clock cavity, collisions between cold atoms shift the phase of their coherence producing a frequency shift of the clock. To measure this frequency shift, we vary the atomic density on successive fountain launches and look for a relative shift of the Ramsey fringes. In Fig. 3 we show a series of

measurements of the frequency as a function of density (circles) for atoms prepared in both $|1,0\rangle$ and $|2,0\rangle$. The extrapolated shift for a density of $1.0(6)\times 10^9$ cm^{-3} is $-0.38(8)$ mHz.^{8,9} We also show the shift for Cs which is fractionally 30 times larger.³ The measured shift agrees with that calculated in Ref. [5] and also a recent reanalysis of the ^{87}Rb interactions.^{10,11}

The measured frequency differences in Fig. 3 have a precision of $\pm 2\times 10^{-15}$. At the 10^{-15} level, there are several potential error sources. The only source that is explicitly density dependent is the pulling of the transition frequency by the coupling of the atoms to the microwave cavity.¹² In NMR, the effect is known as radiation damping where the field radiated by the magnetization of the sample builds up in the microwave cavity and causes the Bloch vector to decay.¹³ In hydrogen masers, it is called cavity pulling and is used to cancel the collisional frequency shift.¹⁴ Here, more apparent than the decay of the atomic coherence is a small phase shift. When the cavity is detuned from the atomic transition frequency, the field radiated by the atoms is phase shifted relative to the applied field. The Bloch vector precesses about the total field leading to a phase error proportional to $\mu_0\hbar\mu_B^2 N\omega\delta/(\delta^2+\Gamma^2)V_{\text{cav}}$.^{15,16} Here, N is the number of atoms, ω is the transition frequency, δ is the cavity detuning, Γ is the cavity HWHM, V_{cav} is the effective cavity volume, and μ_B is the Bohr magneton.

In Fig. 3 we also show the measured density dependent frequency shift when we detune the clock cavity by $\pm\Gamma$ for atoms prepared in $|1,0\rangle$ (diamonds and squares). The cavity detuning can significantly influence the density dependence. By detuning the cavity, we cancel the cold collision shift.¹⁶ This spin-exchange tuning¹⁴ has advantages for insuring immunity to long-term variations in the number of trapped atoms. Moreover, density extrapolations can be more accurate since the extrapolation does not depend on accurate density ratios.⁴

The cavity pulling has several unique dependences that we observe. For example, the

cavity pulling not only reverses with the cavity detuning δ but also with the initial population inversion of $|1,0\rangle$ and $|2,0\rangle$. In addition, the cavity pulling depends on the transition probability during each cavity passage. For a 0.5 transition probability on the first interaction ($\pi/2$ pulse), a positive cavity detuning δ pulls the frequency higher (lower) for atoms prepared in $|2,0\rangle$ ($|1,0\rangle$). On the second $\pi/2$ pulse, if the microwave frequency is tuned to the side of a Ramsey fringe, the microwave field is phase shifted by $\pi/2$ so that it is parallel or anti-parallel to the Bloch vector. Therefore, the Bloch vector does not precess and the cavity pulling has no first order effect during the second interaction. For a transition probability of 0.25 in the first passage (0.33π pulse), the cavity pulls in the same direction during both cavity passages since the Bloch vector precesses during both. However, the effect of the second passage is small because the number of atoms is 8 times less due to their ballistic expansion. For a transition probability of 0.75 (0.67π pulse), the first cavity passage has a small effect as the Bloch vector is first perturbed in one direction as it precesses to $\theta=\pi/2$ and then the direction of the perturbation reverses once there is a population inversion. On the second passage, the perturbation remains reversed so that the total cavity pulling is small.

We show the cavity pulling effects in Fig 4. We plot the density dependent shift versus the atomic transition probability during the first cavity passage for $n=10^9 \text{ cm}^{-3}$. For a cavity tuned below the atomic resonance, $\delta=-\Gamma$, and atoms prepared in $|1,0\rangle$, the frequency shift is positive and large for a small transition probability (open squares and dashed line). When the atoms are prepared in $|2,0\rangle$, the filled squares show a large negative density dependent shift for a small transition probability. The dotted line and open (filled) diamonds show the opposite density dependence for $\delta=+\Gamma$, and $|1,0\rangle$ ($|2,0\rangle$) state preparation.

To model the data in Fig. 4, we account for the different cold-collision frequency shifts λ_{10} and λ_{20} due to the $|1,0\rangle$ and $|2,0\rangle$ populations, and

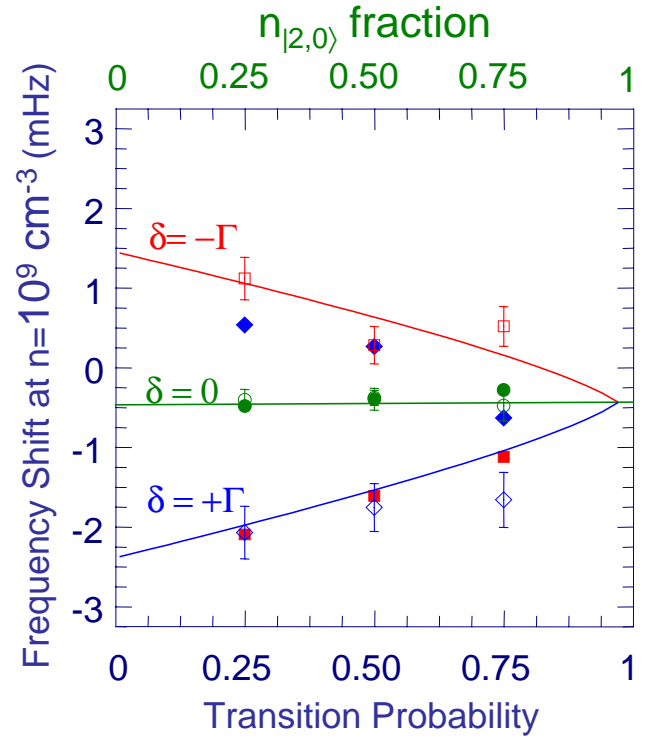


Figure 4. Density dependent shift versus transition probability on a single clock cavity passage for clock cavity detunings of $\delta=+\Gamma$ (diamonds and dotted) and $-\Gamma$ (squares and dashed line). Open (filled) data points are for atoms prepared in $|1,0\rangle$ ($|2,0\rangle$). For $\delta=0$, the circles and solid line are plotted versus the fraction of atoms in $|2,0\rangle$ in the fountain, giving the individual shift contributions from $|1,0\rangle$ and $|2,0\rangle$ state populations. Typical error bars are shown for open points.

the cavity pulling. For no cavity pulling ($\delta=0$), we see essentially no shift as a function of the population in $|2,0\rangle$ during the precession time. We model the 18 measurements in Fig. 4 accounting for the partial frequency shift cross sections and the cavity pulling by integrating the time evolution of the Bloch vector as the atom passes through the microwave field profile of the clock cavity. The model agrees and we find $2(\lambda_{10}-\lambda_{20})/(\lambda_{10}+\lambda_{20})=0.1(6)$. This constrains a determination of the ^{87}Rb interactions that suggests either -1.63 or 0.08 .¹⁰

Although cavity pulling and the cold collision shift are the only systematic errors that explicitly depend on the atomic density, it is important to control all errors near the level of 10^{-15} . Our frequency reference is an ovenized 5 MHz quartz

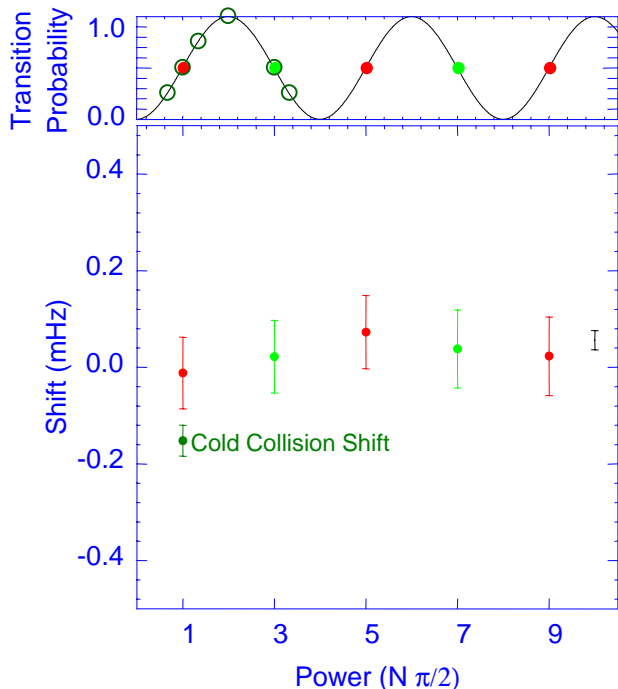


Figure 5. Selection Transition probability (for changing the density) and clock frequency versus power to the selection microwave horn. The fitted uncertainty is shown (rightmost point). After dividing it by 8, it is negligible when compared to the measured collision shift. For the collision shift measurements, we select atoms with a variety of pulses from 0.33π to 1.7π (open circles in the upper graph) to further reduce any inhomogeneous selection effects.

BVA oscillator that is successively frequency multiplied and mixed with a low frequency synthesizer to make 6834.6 MHz. Considerable care is taken to avoid line pulling by spurious frequencies and 60 Hz phase modulation.¹⁷ We test for line pulling and microwave leakage by observing the clock frequency while driving $\pi/2$, $3\pi/2$, ..., $11\pi/2$ pulses and also adjust the fringe space to be most sensitive to 60Hz harmonics. These effects are below 8×10^{-16} and the density dependent component is below 1×10^{-16} .

Inhomogeneities in the state preparation can combine with other errors, such as the distributed cavity phase shift, to mimic a density-dependent frequency shift. To exaggerate this effect, we select atoms with $\pi/2$, ... $9\pi/2$ pulses from the microwave horn as shown in Fig. 5. Thus, any small gradient in the selection would be 8 times larger for a $9\pi/2$ than for $\pi/2$ selection. We fit the

measured frequencies versus $N\pi/2$ to a mean frequency and an alternating term proportional to N . For a $\pi/2$ pulse, the shift is less than 7×10^{-16} . Further, we take data by selecting 1/4 of the atoms with both 0.3π and 1.7π pulses so that any selection gradient is reversed.

Another spatially inhomogeneous shift is the quadratic Zeeman shift from the 710 μG bias field. The shift of the clock's frequency is 4.3×10^{-14} . Over the top 4 cm of the fountain, the field is homogeneous over the volume sampled by the atoms to 1 μG and the gradient is less than 20 $\mu\text{G}/\text{cm}$ producing systematic errors less than 1×10^{-16} . Finally, we check for an AC Stark shift due to the lasers and find the density dependent component to be below 2×10^{-16} .

The atomic density is measured using laser absorption. An attenuated 1mm laser beam is apertured, aimed vertically through the center of the clock cavity, and then centered on the ball of atoms. We frequency scan a 50 μs pulse over 40 MHz near the $2 \rightarrow 3'$ transition at 9 times throughout the fountain trajectory. We measure the vertical size of the atomic sample on the upward and downward passages through the detection region, with and without state preparation. We model the evolution of the atomic density as a ballistic expansion of uncorrelated Gaussian velocity and spatial distributions and account for the heat added during the state preparation. This produces a density as a function of time as shown in Fig. 6. We calculate the time-averaged density for the atoms that we detect below the clock cavity (dashed line in Fig. 6). This effective density depends on the transverse velocity and spatial distributions, and we extract this information from the time evolution of the vertical optical thickness of the sample. Without independent corroboration, it is difficult to be certain about the absolute density scale to better than 60%. With quantitative and absolute tests of our model of cavity pulling, the cavity pulling could be used to measure accurately and independently the atomic density.¹⁸

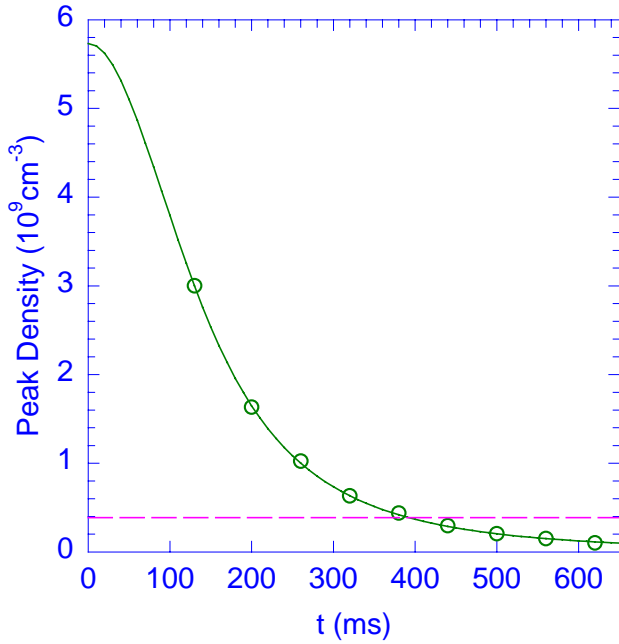


Figure 6. Peak transverse density as a function of time. The temporally and spatially averaged density is shown as a dashed line.

We tune the clock cavity by $\delta=\pm\Gamma$ by changing its temperature by $\mp 2.5\text{K}$. To measure the frequency response of the cavity we detect the AC Zeeman shift of the clock states due to a strong microwave sideband that is injected into the clock cavity.⁶ In Fig 7, we show the shift of the clock transition (inset) and the inferred response of the cavity. The loaded Q of our TE_{102} copper clock cavity is 13,000 and it is tuned with an accuracy of 5 kHz.

3. JUGGLING CLOCKS

One can achieve higher stabilities and eliminate the dead time (reducing the requirements for the local reference oscillator) by *juggling* atoms in the fountain as shown in Fig. 8. With a $S/N = 2300$ on a single launch, the frequency uncertainty would be $\delta\nu/\nu = \Delta\nu/(\pi \nu S/N) = 2 \times 10^{-14}$. If the cycle time is 1 s, then the fractional instability of the clock after 1s of averaging is $\sigma_y(\tau=1\text{s}) = 2 \times 10^{-14} \tau^{-1/2}$. By launching balls of atoms at a rate of 25 s^{-1} , the dead time is eliminated and gives a short-term instability of $\sigma_y(\tau) = 4 \times 10^{-15} \tau^{-1/2}$. This

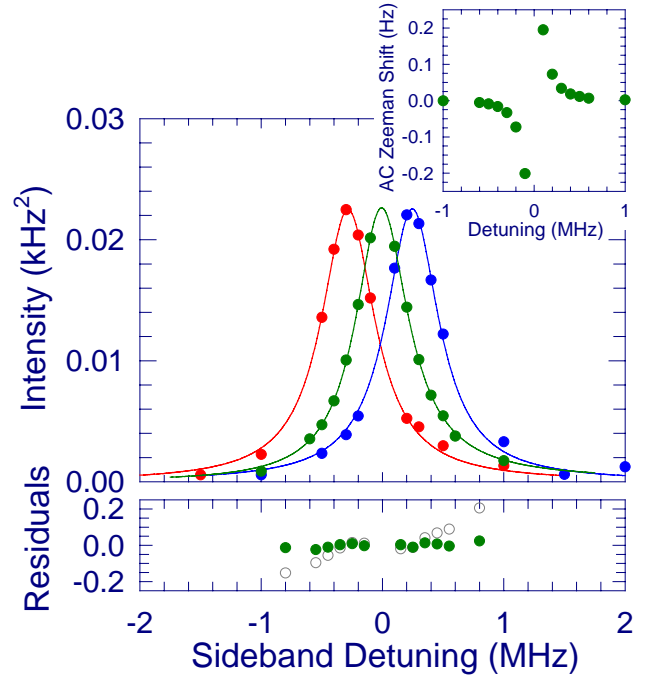


Figure 7. Cavity response versus sideband frequency for 3 temperatures. The cavity response is measured using the AC Zeeman shift of the clock transition due to a microwave sideband (inset). The residuals of the $\delta=0$ fit have an asymmetry due to the TE_{101} waveguide feed cavity (open circles). Accounting for it, the residuals are 1% or 0.04 dB (filled circles).

improvement is achieved without the technical difficulty of higher S/N and higher atomic densities. There are 2 important problems: 1) shutters, as shown in Fig. 8, must be used to block the trapping and cooling light from the interrogation region of the clock; 2) collisions

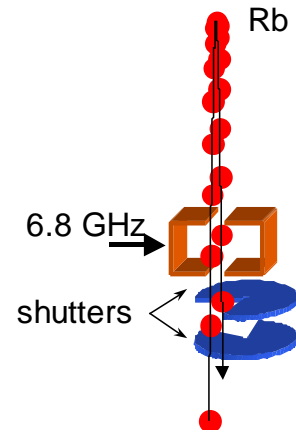


Figure 8. Schematic for a juggling fountain clock. Balls of laser-cooled atoms are launched faster than the flight time above the microwave cavity.

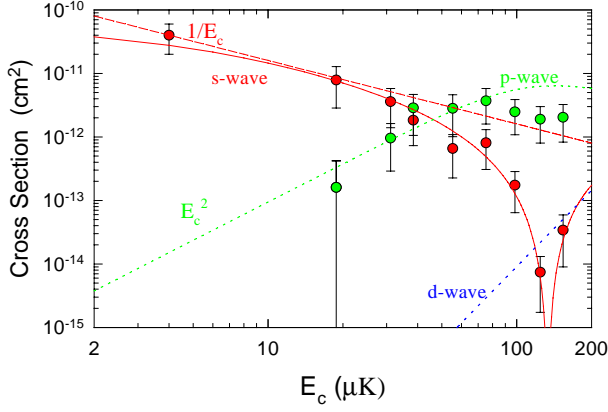


Figure 9. Energy dependence for s & p-waves cross sections. For reference, we show lines corresponding to $1/E$ and E^2 corresponding to an s-wave resonance and the p-wave quantum scattering threshold. At higher energies, the s-wave cross section goes to zero indicating a Ramsauer-Townsend minimum near 200 μK .

between juggled balls of atoms will shift the frequency of the clock.

We have demonstrated a juggling Cs fountain and have studied collisions between 2 balls of atoms.¹⁹ In this experiment we observe the velocity changes rather than a phase shift of an atomic coherence. We rapidly launch 2 balls of atoms from a double-MOT²⁰ at the same velocity. The relative velocity is then $v_r = \Delta T \times g$ where ΔT is the delay between launches. Here, $\Delta T = 7 \text{ ms} \rightarrow 20 \text{ ms}$ corresponds to collision energies of 19 to 150 μK . This range of energies is interesting as one expects to see the p-wave quantum scattering threshold – at low energies only s-wave scattering occurs since, for impact parameters that are within the range of the interatomic potential, the velocity is low enough that the angular momentum is less than \hbar . As the energy increases to about 30 μK , there is enough angular momentum for impact parameters within the potential to have $\ell=1$.²¹

To be sensitive to the differential cross section, we detect the vertical velocity component of the scattered atoms using a 2-photon Raman transition.^{20,22} In Fig. 9, we show the Cs s & p-wave cross-sections as a function of energy. At low energies, the s-wave cross section, which is

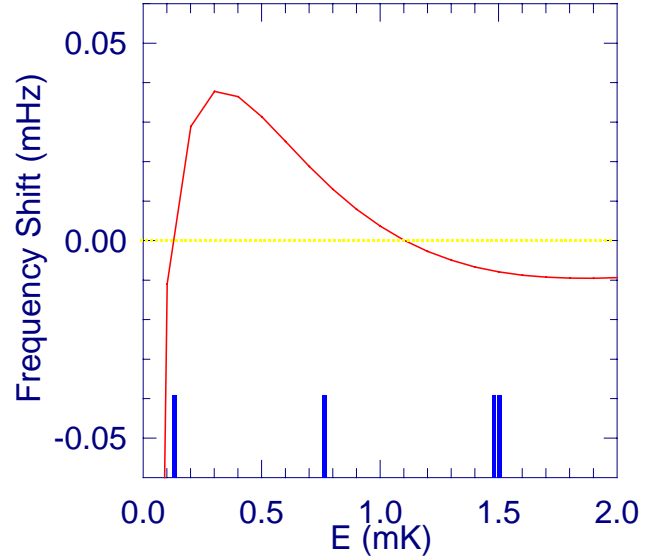


Figure 10. Juggling frequency shift for s-waves. The juggling shift is zero for time delays of 22ms (0.12mK) and 66 ms (1.1mK). The energy spectrum shown corresponds to juggling pattern depicted in Fig. 11.

pure triplet scattering, becomes constant. The p-wave cross section increases as the square of the energy for low energies as expected for a p-wave scattering threshold and then rolls over at higher energies. Since the p-wave channel is an admixture of singlet and triplet interactions, we can get a great deal of detailed information about the Cs-Cs scattering at low energies. The s-wave data determines the triplet potential allowing the p-wave to determine the singlet. This experiment is the first to resolve the quantum scattering for atomic partial waves.

At higher energies, the s-wave cross section decreases to nearly zero indicating a s-wave Ramsauer-Townsend cross-section minimum²³ near 200 μK . The Ramsauer-Townsend effect can be used to minimize the cold collision shift in a juggling fountain clock. By carefully choosing the launch rate, one can minimize the effects of collisions between successive balls

In Fig. 10 we show a calculation of the s-wave juggling frequency shift for ^{87}Rb . The first null in the shift occurs at 0.12 mK corresponding to a time delay of 22 ms. Unfortunately, the peak of the s-wave juggling shift is very nearly at a time delay of 44 ms. Therefore, for a juggling rate of $1/(22 \text{ ms})$, the energy for collisions

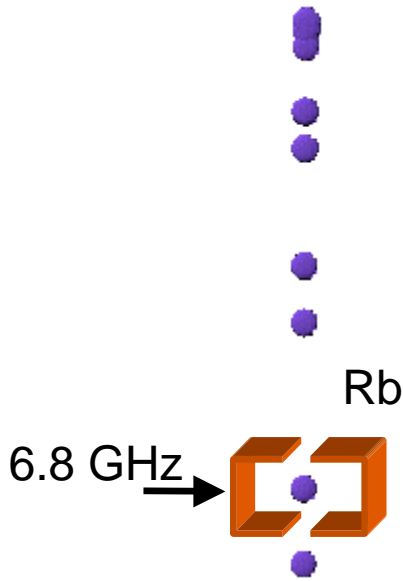


Figure 11. Juggling pattern of alternate launch delays of 22 and 55 ms to cancel the s-wave juggling frequency shift.

between every other ball would be near the peak of the juggling shift. To cancel the juggling shift, one can launch with a more sophisticated pattern. A pattern that cancels the s-wave shift launches balls with alternate delays of 22 and 55 ms as shown in Fig. 11. The energy spectrum for this pattern is also shown in Fig. 10. Each ball collides with 1 ball with a 22 ms delay for which there is no shift. Each ball also collides with another at 55 ms delay, for which the shift is positive, and with 2 balls at 77 ms where the shift is negative and half as large as the shift at 55 ms. There is no p-wave shift due to Bose symmetry and higher partial waves will generally have random signs and all of the shifts decrease at higher energies. It is likely that a pattern similar to that in Fig. 11 will give a high juggling rate and cancel the total juggling collision shift.

4. COLD-COLLISION FREQUENCY-SHIFT IN MICROGRAVITY

As in fountains, the frequency shift due to cold collisions³ plays an important role in the design of a microgravity clock. For RACE, we have chosen Rb because of its small cold collision shift. One might naively expect that the

cold collision shift is much less in microgravity since the interrogation time is so long and therefore the atoms spread out and have a much lower density. However, the requirement that the stability be high enough so that the accuracy is achieved in 1 day of averaging (10^5 s) demands high S/N, and therefore the collision shift is non-negligible.

It is interesting to examine the scaling of the cold collision shift with the interrogation time T with a fixed physical size of the clock and also demanding the same short-term stability. The fractional stability for 1 s of averaging is $\frac{\delta\nu}{\nu} = \sigma(\tau=1s) = \frac{\Delta\nu}{\pi\nu S/N}$ where S/N is the signal to

noise, ν is the transition frequency, and $\Delta\nu$ is the transition linewidth. If the S/N is limited by shot-noise, then $S/N = \sqrt{N} = \sqrt{n_f A \frac{L}{T}(1s)}$ where N is the number of detected atoms, n_f is the final atomic density, A is the area of the cavity aperture, and L is the length of the interrogation region. Given the equation for the instability at 1 s, we then get $n_f = \frac{1}{[2\pi\nu\sigma(1s)]^2 ALT(1s)}$. Assuming that the source

is 20 cm from the cavity and the cavity is 50 cm long, this geometry implies that the average density is 7.8 times the final (for interrogation times of 3-100s). Therefore, the collision shift, for a fixed length and short-term stability, scales as $1/T$ so that the long interrogation times in microgravity helps to decrease the frequency error due to cold collisions.

Specifically, with $T=10s$, a short-term stability of $\sigma_y(\tau) = 3 \times 10^{-15} \tau^{-1/2}$ requires $S/N = 600 \tau^{-1/2}$, which is not technically challenging. This implies that 0.4×10^6 Cs atoms/s are detected and, with a 1.1 cm microwave cavity aperture and a 5 cm/s launch velocity, the *final* density is $n_f = 7 \times 10^4 \text{ cm}^{-3}$, and the average density $n = 6 \times 10^5 \text{ cm}^{-3}$ producing a cold collision shift of -1.4×10^{-15} . This can be extrapolated to an accuracy of about $\pm 1 \times 10^{-16}$. Using the same length, interrogation time, and short-term stability for ^{87}Rb , we get a collision shift of -3×10^{-17} collision which can be cancelled by spin

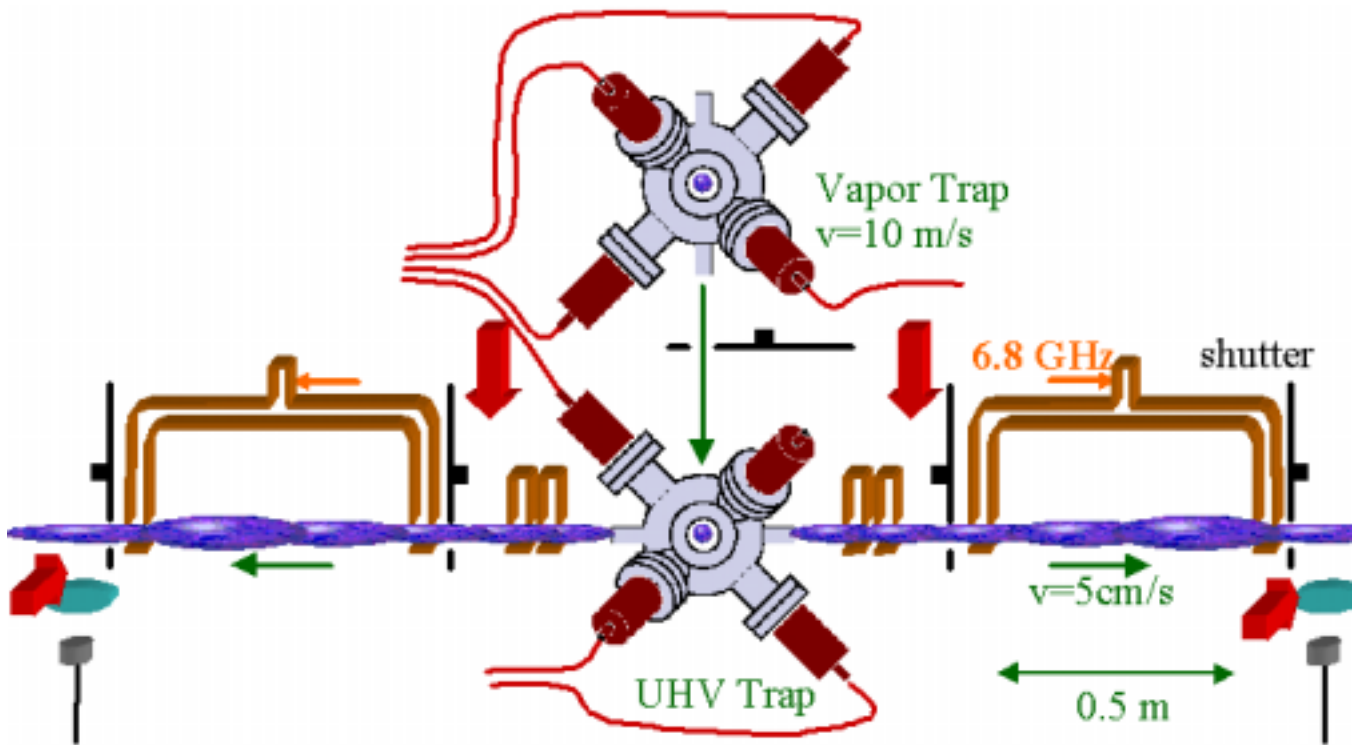


Figure 1. Schematic for juggling microgravity Rb clock RACE. The double MOT launches atoms at high speed from the (upper) vapor trap to the (lower) UHV trap so that the shutter between the traps can be nearly always closed. The shutters between the UHV trap and the cavities are nearly always open except during the ≈ 5 ms that the light for the UHV trap is turned on. The atoms are alternately launched left or right to go through one clock cavity or the other.

exchange tuning with a likely uncertainty less than 10^{-17} .⁸

5. COMPARISON OF MICROGRAVITY RB AND CS CLOCKS

Given that the collision shift is much smaller for ^{87}Rb than for Cs, it is interesting to compare the potential performance of Rb and Cs clocks in microgravity. One of the important differences is the smaller hyperfine transition frequency of ^{87}Rb . For terrestrial fountains the linewidth is essentially fixed at 1 Hz and a 30% lower line Q for ^{87}Rb has some impact on the clock's performance. In microgravity, a $T=10$ s interrogation time implies a very high Q of 1.4×10^{11} . On earth, increasing the Q is difficult as the fountain height increases as T^2 whereas in microgravity, the length of the clock only increases linearly (or not at all if the launch velocity is reduced).

The short-term stability is also not adversely affected by the lower hyperfine frequency ν . For a lower ν , the size of the hole in the cavity can be larger so that the area increases as ν^{-2} . Therefore the shot-noise-limited S/N scales as ν^{-1} so that the stability is independent of ν . One could argue that the lower transverse velocities achievable with Cs, as compared to Rb, allow 3 times as many atoms to be detected. However, for both cases, one can easily have enough phase space density to reach a short-term stability of $\sigma_y(\tau) = 1 \times 10^{-15} \tau^{-1/2}$ so that the important limitation to the stability of a Cs clock is that the density must be reduced to manage the cold collision shift.

6. STABILITY OF MICROGRAVITY CLOCKS

If we launch a single ball of ^{87}Rb atoms through the microgravity clock (see Fig. 1), we can calculate the uncertainty in the frequency.

Here, for an interrogation time $T = 10$ s, we detect 10^6 atoms so that the signal-to-noise S/N is 10^3 .

$$\frac{\delta\nu}{\nu} = \frac{\Delta\nu}{\pi\nu S/N} = 2.3 \times 10^{-15}$$

Launching a ball of atoms approximately every $T = 10$ s gives an Allan variance of

$$\sigma_y(\tau) = \frac{\Delta\nu}{\pi\nu S/N} \sqrt{\frac{T}{\tau}} = 7.3 \times 10^{-15} / \sqrt{\tau}.$$

Since $\Delta\nu$ and S/N both scale as $1/T$, the Allan variance is proportional to $T^{1/2}$. This seemingly presents a serious problem if we require higher stability to achieve the high potential accuracy of microgravity clocks.

Multiply launching balls of atoms, or juggling,¹⁹ allows one to reclaim the high stability potential of a microgravity clock. By launching atoms at a rate $R = 5 \text{ s}^{-1}$, the stability is

$$\sigma_y(\tau) = \frac{\Delta\nu}{\pi\nu S/N \sqrt{R\tau}} = 1 \times 10^{-15} / \sqrt{\tau}$$

which is independent of the interrogation time T . This clearly indicates the importance of juggling to achieve high stability and accuracy in laser-cooled microgravity clocks.

7. DESIGN OF JUGGLING CLOCKS AND RACE

Multiple launching imposes several constraints on the design of a microgravity clock. Shutters are needed to block the light scattered from trapping, state preparation, and detection from the interrogation region. In Fig. 1, we show a design for a juggling microgravity clock that has a pair of shutters surrounding the Ramsey cavity. This is a design for our Rb microgravity clock, RACE. First we discuss the laser trapping and cooling techniques and then the advantages of have 2 clock cavities.

The double-MOT^{19,20} allows a high throughput of cold atoms and therefore a high short-term stability. The high throughput is possible as the double-MOT can rapidly capture many cold atoms and then efficiently launch them

through the Ramsey cavity. The “upper” vapor cell trap in Fig. 1 essentially continually traps atoms and then launches them at 5-10 m/s to the UHV trap “below.” Because of the high launch velocity from the vapor cell trap, the atoms pass quickly through the shutter separating the 2 traps. This implies that the shutter only needs to open for the short time the ball of atoms flies through and, only during that time, the lasers for the vapor-cell trap must be extinguished (so that no laser light enters the interrogation region).

The real advantage of the double-MOT design is that the UHV trap can capture and launch a ball of atoms in as little as 5 ms. This implies that the shutter separating the UHV trap and interrogation region only has to close for 5 ms for each launch and therefore is nearly always open. This allows a high throughput since, if the shutter is ~ 10 cm from the center of the UHV trap, the ball of atoms will have expanded considerably before reaching the shutter. For our juggling Cs experiment,¹⁹ it was crucial to reduce the trapping and cooling time of the UHV trap be able to study collisions at low energies (juggling rates as high as 140 s^{-1}).

One also has to worry about the effect of the trapping light on the previously launched ball of atoms from the 2nd trap. Again, this was a crucial step in our Cs juggling experiment. By “hiding” the ball in the lower hyperfine state immediately after the launch, and by carefully controlling the low intensity repumping light to the 2nd trap, we can capture and launch balls of atoms essentially on top of one another.¹⁹

The RACE schematic in Fig. 1 shows 2 clock cavities. After atoms are collected in the lower laser trap, they are launched either through one cavity or the other. Having 2 cavities is important for a number of reasons which we discuss below. One advantage is that it greatly reduces the requirements for the local oscillator. Few oscillators can perform at the $\sigma_y(\tau) = 3 \times 10^{-15} \tau^{-1/2}$ level and there is significant work required to develop their flight worthiness. The essential problem with only a single cavity is that the microwave frequency fed to the cavity must be changed from one side of the transition to the other. During the switchover, all of the atoms

must be cleared from the cavity and this means the oscillator is not tracked for about 10s when $T = 10$ s. With 2 cavities, we can do the switchover for one cavity while still monitoring the oscillator with the other cavity and therefore the stability of the clock isn't compromised by the local oscillator's instability.

Vibrations on the ISS in the direction of the launch velocity will cause a noise in the interrogation time. With 2 cavities, the 2 detected signals will behave oppositely so that the effects of vibrations can be identified, correlated with an accelerometer, and removed.

One of the largest systematic errors is the AC Stark shift due to Blackbody radiation at 300K. A measurement of the red shift and time dilation with frequency inaccuracies of 10^{-17} demands absolute knowledge of the average temperature in the clock cavity at the 0.01K level. Having 2 cavities will allow a critical check on our accuracy evaluation.

In addition, having 2 cavities gives important redundancy. For example, if a shutter fails, we will still be able to achieve mission success goals (although require longer averaging times).

8. CONCLUSIONS

We have demonstrated a prototype of an ^{87}Rb fountain clock. Varying the density, we see a small shift in the clock frequency that is fractionally 30 times smaller than the shift for a laser-cooled Cs clock. By detuning the microwave clock cavity, we cancel the shift. This will allow an ^{87}Rb fountain clock to operate with a short-term stability of 2×10^{-14} for 1s of averaging with a cold collision shift of 2×10^{-16} that can be cancelled with an accuracy of 1×10^{-17} . Juggling atoms will increase the stability to 4×10^{-15} for 1s of averaging, giving an unprecedented combination of short-term stability and long-term accuracy. We have demonstrated a juggling Cs atomic fountain and observed the energy dependence for s & p-wave scattering, including the Ramsauer-Townsend effect. In a juggling fountain clock, we can choose the

juggling rate and pattern to utilize the Ramsauer minima so that the juggling frequency shift can be cancelled.

To achieve the potential accuracy of laser-cooled microgravity clocks with reasonable integration times, atoms must be multiply launched (juggled). The short-term stability is proportional to the launch rate and this in turn implies that high accuracy and stability favor long interrogation regions. Laser-cooled microgravity clocks can achieve short-term stabilities approaching $\sigma_y(\tau) = 3 \times 10^{-15} \tau^{-1/2}$. At this stability, the largest error in a Cs microgravity clock is the cold collision frequency shift. By using ^{87}Rb , the collision shift is 30 times smaller allowing an accuracy of 10^{-17} . We propose a design using a double-MOT and 2 cavities which simplifies the trapping and shutter design while maintaining a high throughput of cold atoms, minimizes the local oscillator requirements, eliminates vibrations, and provides failure and accuracy redundancy.

9. ACKNOWLEDGEMENTS

We acknowledge discussions with Servaas Kokkelmans, Boudewijn Verhaar, and Mike Hayden and financial support from the NASA Microgravity program, an NSF NYI award, and a NIST Precision Measurement Grant.

10. REFERENCES

1. See K. Gibble and S. Chu, *Metrologia* **29**, 201 (1993).
2. E. Tiesinga, B. J. Verhaar, H. T. C. Stoof, and D. van Bragt, *Phys. Rev. A* **45**, 2671 (1992).
3. K. Gibble and S. Chu, *Phys. Rev. Lett.* **70**, 1771 (1993).
4. K. Gibble and B. J. Verhaar, *Phys. Rev. A* **52**, 3370 (1995).
5. S. J. J. M. F. Kokkelmans, B. J. Verhaar, K. Gibble, and D. J. Heinzen, *Phys. Rev. A* **56**, 4389 (1997).
6. C. Fertig and K. Gibble, *IEEE Trans. Instr. Meas.* **48**, 520 (1999).
7. S. Bize, Y. Sortais, M. S. Santos, C. Mandache, A. Clairon, and C. Salomon, *Europhys. Lett.* **45**, 558 (1999).

8. C. Fertig and K. Gibble, Phys. Rev. Lett. **85**, in press (2000).
9. See also S. Bize, Y. Sortais, C. Mandache, A. Clairon, and C. Salomon, submitted to Phys. Rev. Lett (2000).
10. S. Kokkelmans and B. J. Verhaar, private communication (2000).
11. Carl Williams, private communication (2000).
12. There is cavity pulling in Cs beam clocks due to the variation of the microwave power across the transition. This effect is easily eliminated in fountain clocks by working with $2\pi/2$ pulses and measuring more than the central Ramsey fringe.
13. S. Bloom, J. Appl. Phys. **28**, 800 (1957).
14. S. B. Crampton, Phys. Rev. **158**, 57 (1967).
15. M. E. Hayden and W. N. Hardy, J. Low Temp. Phys. **99**, 787 (1995).
16. C. Fertig, J. Bouttier, and K. Gibble, to be submitted to IEEE Trans. Instr. Meas.
17. A. De Marchi, G. D. Rovera, and A. Premoli, Metrol. **20**, 37 (1984).
18. Our cavity pulling model and our measured density are consistent to 10% with an uncertainty of at least 30%.
19. R. Legere and K. Gibble, Phys. Rev. Lett. **81**, 5780 (1998).
20. K. Gibble, S. Chang, and R. Legere, Phys. Rev. Lett **75**, 2666 (1995).
21. See P. S. Julienne and F. H. Mies, J. Opt. Soc. Am. B **6**, 2257 (1989).
22. M. Kasevich, D. S. Weiss, E. Riis, K. Moler, S. Kasapi, and S. Chu, Phys. Rev. Lett. **66**, 2297 (1991).
23. Ramsauer, Ann. der Physik **72**, 345 (1923); Townsend and Bailey, Phil. Mag. **43**, 593 (1922).

Towards Precision Experiments with Bose-Einstein Condensates

Todd L. Gustavson[†] and Wolfgang Ketterle

*Department of Physics and Research Laboratory of Electronics,
Massachusetts Institute of Technology, Cambridge, MA 02139, USA*

As a source of ultra-cold coherent matter, Bose-Einstein condensation (BEC) in dilute atomic gases has had great impact on the field of atom optics, and should enable substantial improvement in future precision measurements. Understanding the effects of atomic interactions and collective behavior within condensates provides a foundation for future measurements utilizing BEC. We recently demonstrated that a condensate can be used to amplify matter waves. Matter wave amplifiers may be used to improve signal-to-noise or to build active atom interferometers; for example, the analog of optical ring laser gyroscopes. We have studied superfluid suppression of collisions using impurities generated by two-photon Raman transitions. We are building a third BEC apparatus that should allow us to use optical tweezers to move condensates into a separate “science chamber” where experiments requiring greater optical and mechanical access may be conducted. Large volume optical dipole traps can be used to capture large numbers of atoms with low densities, long lifetimes and low mean-field shifts. They can be used instead of magnetic traps to support atoms against gravity (including atoms in magnetic field insensitive sublevels), which may be useful for a variety of studies in anticipation of future microgravity experiments.

I. ULTRA-COLD ATOMS AND MICROGRAVITY

The development of laser-cooling techniques for atoms has led to dramatic improvements for many types of experiments by increasing interrogation times and detection signal-to-noise ratios. These techniques have been utilized in experiments such as state-of-the-art atomic clocks [1], precision measurements such as \hbar/m [2] (determines the fine structure constant α), and for inertial force measurements: namely gravitational gradients and acceleration [3], and rotation rates [4]. Gravity typically limits interrogation times in such measurements to ≤ 1 sec (i.e., for a fountain with ~ 1 m height). Experiments in microgravity could overcome these limitations; however, atoms from typical laser-cooled sources such as a magneto-optic trap (MOT) still spread out with velocities of order a few cm/sec, imposing a practical limit on the interrogation time because the signal-to-noise decreases as the atomic cloud expands. Ultra-cold atoms from an adiabatically expanded BEC are the obvious solution for the next generation of microgravity atomic physics experiments, and may result in 1000-fold longer interrogation times than ground-based experiments with conventional laser-cooled sources, yielding substantial improvements in sensitivity. More sensitive atom interferometers could lead to improved precision measurements of certain fundamental constants, higher resolution for the Global Positioning System (GPS), and tests of general relativity.

[†]Electronic address: TLG@MIT.edu

Our group has developed a variety of tools for manipulating and probing condensates which may be useful for precision measurements. For example, an optical dipole trap (ODT), or laser tweezers, formed by focusing a red-detuned laser beam, can be used to trap condensates. Such a trap can achieve long storage lifetimes and can be used to manipulate atoms with μm precision.

Matter wave amplifiers have been created using a condensate [5, 6] by preparing it with an appropriate laser beam. The amplifier accepts an input seed pulse of atoms and outputs a proportionately larger number of atoms that are phase-coherent with the input pulse. This technique has been used to create an active interferometer, in which a matter-wave amplifier is inserted into one or both arms of an interferometer. Active atom interferometers may be advantageous for certain experiments just as active ring lasers have improved sensitivity of optical gyroscopes [7].

We have also studied collisions and superfluidity within the condensate. Atom lasers are likely to be useful sources for atom interferometry and lithography; however, normally the atoms coupled out of the condensate collide with the atoms at rest, introducing loss. By adjusting the speed of sound, c , in the condensate via the density, one can reach a superfluid regime where atoms moving through the condensate at velocity $v \leq c$ do not undergo collisions. Therefore, this method constitutes a superfluid output-coupler. A continuous atom laser would also be desirable for many purposes, and this may be achievable by transporting condensates with an ODT to load multiple condensates into a second trap.

The remaining sections of this paper will describe the experiments we have recently conducted to study the tools mentioned above.

II. LARGE VOLUME OPTICAL DIPOLE TRAPS

Trapping of condensates in an ODT with cylindrical symmetry was demonstrated by our group previously [8]. An important advantage of the ODT is that it can be used to trap atoms in any state (or mixtures thereof), unlike magnetic traps that trap only states that minimize energy for weak magnetic fields. Because condensates have such low energy, little optical power is needed – typically on the order of a few mW. Currently, we are using a solid state laser operating at 1064 nm, far to the red of the sodium transition resonances at 589 nm. The Raleigh scattering rate (absorption and spontaneous emission) is proportional to I/Δ^2 , where I is the laser intensity and Δ is the detuning. However, the trap potential depth is proportional to I/Δ . Therefore, using a large detuning, it is possible to achieve sufficient trap depth with negligible photon scattering. Due to gravity, the trapping laser must be tightly focused to provide a steep potential gradient and a strong restoring force to support the atoms.

We have used cylindrical lenses to form optical traps with aspect ratios between 25 and 50 to 1. The light is tightly focused vertically to support against gravity but the trap is only weakly confining transversely. This yields a pancake-shaped trap with much larger volume than a conventional ODT, with correspondingly lower atomic densities of order $1 \times 10^{14} \text{ cm}^{-3}$. At low density, loss due to collisions is greatly reduced, increasing the lifetime of trapped atoms to tens of seconds or more. The laser beam waist in the tightly focused vertical direction is currently about $15 \mu\text{m}$.

The ability to hold atoms in a weak trap for long times is a useful preliminary step for certain studies in anticipation of future microgravity experiments. We have done preliminary experiments using RF transitions to transfer condensates from the $|F = 1, m_F = -1\rangle$ state, in which they are produced, to $|F = 2\rangle$ states with various m_F values. By measuring trap lifetimes and observing the atoms with time of flight imaging, we hope to compare the scattering lengths of the $|F = 1\rangle$ and $|F = 2\rangle$ states. We have recently driven the clock transition, namely $|F = 1, m_F = 0\rangle \rightarrow |F = 2, m_F = 0\rangle$, using an RF transition.

The laser light comprising the ODT can be easily manipulated; for example, acousto-optic modulators can be used to scan the light in one or two dimensions or modulate it in time. This makes it possible to generate custom potentials with nearly arbitrary shape. However, preliminary experiments indicate that extremely high scan rates are required to avoid heating. It should be possible to study condensates in restricted dimensions, effectively in either 1D or 2D, by using small numbers of atoms in an ODT.

Finally, we can use the ODT to transport condensates by shifting the focus of the laser beam. The lens system we use to generate our ODT uses a computer controlled translation stage to move one of the final lenses. By controlling the acceleration of the stage, we should be able to move the condensate about 25 cm in a few seconds while keeping the atoms in the ground state of the trap. We plan to use this technique to move condensates from the trapping chamber of a new BEC apparatus into a connected “science chamber,” which will have improved optical access. The science chamber may be valved off from the UHV trapping chamber and rapidly reconfigured for performing various experiments. We have tested the ODT transport in our original BEC apparatus and successfully moved condensates up to ~ 4 cm, limited only by the size of the current chamber. Our new apparatus is now fully assembled and was recently evacuated.

III. AMPLIFICATION OF LIGHT AND ATOMS IN A BOSE-EINSTEIN CONDENSATE

Bose-Einstein condensates illuminated by an off-resonant laser beam (“dressed condensates”) were used to realize phase-coherent amplification of matter waves [5, 6]. The amplification process involved the scattering of a condensate atom and a laser photon into an atom in a recoil mode and a scattered photon. This four-wave mixing process between two electromagnetic fields and two Schrödinger fields became a self-amplifying process above a threshold laser intensity, leading to matter wave gain. (The total number of atoms in the system is conserved, but the BEC acts as a reservoir from which atoms are transferred, maintaining phase-coherence with the seeding pulse of atoms.)

However, the symmetry between light and atoms indicates that a dressed condensate should not only amplify injected atoms, but also injected light. The dressed condensate picture is illustrated in Fig. 1.

We have studied the optical properties of a dressed condensate above and below the threshold for matter wave amplification [9]. The optical gain below the threshold has a narrow bandwidth due to the long coherence time of a condensate. The gain represents the imaginary part of the complex index of refraction. A sharp peak in the gain implies a steep dispersive shape for the real part of the index of refraction $n(\omega)$. This resulted in an extremely slow group velocity for the amplified light. Fig. 2 shows that light pulses were delayed by about $20 \mu\text{s}$ across the $20 \mu\text{m}$ wide condensate, corresponding to a group velocity of 1 m/s. This is one order of magnitude slower than any value reported previously [10].

Above the threshold to matter wave amplification, we observed non-linear optical behavior. Thus we could map out the transition from single-atom gain to collective gain.

IV. SUPERFLUID SUPPRESSION OF IMPURITY SCATTERING

The concept of superfluidity applies to both macroscopic and microscopic objects. In both cases, there is no dissipation or drag force as long as the objects move with a velocity less than the so-called critical velocity. A moving macroscopic object creates a complicated flow field. Above

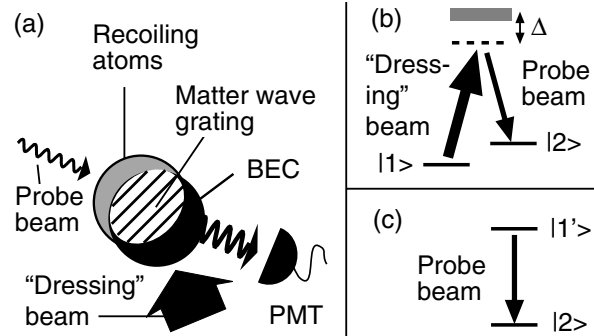


FIG. 1: Amplification of light and atoms by off-resonant light scattering. (a) The fundamental process is the absorption of a photon from the “dressing” beam by an atom in the condensate (state $|1\rangle$), which is transferred to a recoil state (state $|2\rangle$) by emitting a photon into the probe field. The intensity in the probe light field was monitored by a photomultiplier. (b) The two-photon Raman-type transition between two motional states ($|1\rangle$, $|2\rangle$) gives rise to a narrow resonance. (c) The dressed condensate is the upper state ($|1'\rangle$) of a two-level system, and decays to the lower state (recoil state of atoms, $|2\rangle$) by emitting a photon. Since the system is fully inverted, there is gain for the probe beam.

a certain velocity, vortices are created. In contrast, the physics of moving impurities, which are microscopic objects, is much simpler. At velocities larger than the Landau critical velocity, they will create phonon excitations, or rotons in the case of liquid helium-4.

We created impurity atoms in a trapped BEC by transferring some of the atoms into another hyperfine state using an optical Raman transition. The photon recoil and therefore the velocity of the impurity atoms could be varied by changing the angle between the two Raman laser beams. For technical reasons, we instead varied the density to change the speed of sound. Collisions between the impurity atoms and the condensate were observed as a redistribution of momentum when the velocity distribution was analyzed with a ballistic expansion technique. The collisional cross section was dramatically reduced when the velocity of the impurities was reduced below the speed of sound of the condensate, in agreement with the Landau criterion for superfluidity [11]. The results are shown in Fig. 3.

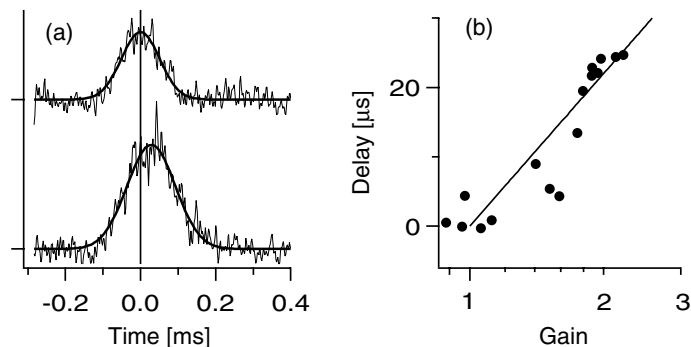


FIG. 2: Pulse delay due to light amplification. (a) Amplification and $20 \mu\text{s}$ delay were observed when a Gaussian probe pulse of about $140 \mu\text{s}$ width and $0.11 \text{ mW}/\text{cm}^2$ peak intensity was sent through the dressed condensate (bottom trace). The top trace is a reference taken without the dressed condensate. Solid curves are Gaussian fits to guide the eyes. (b) The observed delay time was proportional to $\ln(g)$, where g is the observed gain.

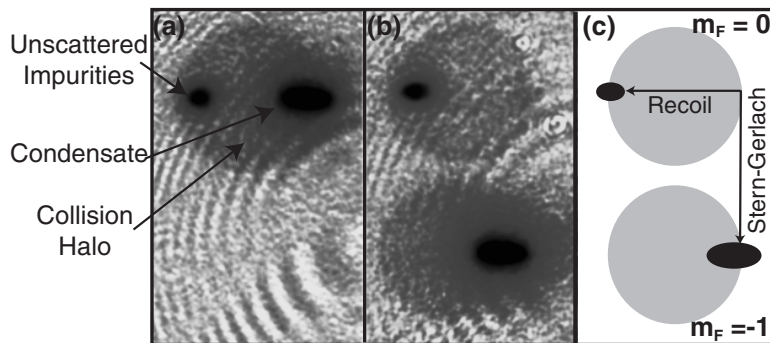


FIG. 3: Observation of collisions between the condensate and impurities. The impurities in the $m_F = 0$ hyperfine state traveled at 6 cm/s to the left. Collisions redistribute the momentum over a sphere in momentum space, resulting in the observed halo (a). In figure (b), the impurities and the condensate in the $m_F = -1$ state were separated with a magnetic field gradient during the ballistic expansion. The effect of collisions is to slow down some of the impurity atoms and speed up the condensate atoms. The absorption images are 4.5 mm times 7.2 mm in size.

In related work, others in our group have recently studied superfluid flow in the macroscopic regime, and measured a density-dependent critical velocity by stirring the condensate with a blue-detuned laser beam [12].

ACKNOWLEDGMENTS

I wish to acknowledge my collaborators: A.P. Chikkatur, A. Görlitz, S. Gupta, S. Inouye, R.F. Löw, and D.E. Pritchard. This work was supported by NASA, ONR, NSF, ARO and the Packard Foundation.

REFERENCES

- [1] C. Santarelli, P. Laurent, P. Lemonde, A. Clairon, A. G. Mann, S. Chang, A. N. Luiten, and C. Salomon, *Phys. Rev. Lett.* **82**, 4619 (1999).
- [2] D. S. Weiss, B. C. Young, and S. Chu, *Appl. Phys. B* **59**, 217 (1994).
- [3] M. J. Snadden, J. M. McGuirk, P. Bouyer, K. G. Haritos, and M. A. Kasevich, *Phys. Rev. Lett.* **81**, 971 (1998).
- [4] T. L. Gustavson, A. Landragin, and M. A. Kasevich, *Class. Quantum Grav.* **17**, 2385 (2000).
- [5] S. Inouye, T. Pfau, S. Gupta, A. P. Chikkatur, A. Görlitz, D. E. Pritchard, and W. Ketterle, *Nature* **402**, 641 (1999).
- [6] M. Kozuma, Y. Suzuki, Y. Torii, T. Sugiura, T. Kuga, E. W. Hagley, and L. Deng, *Science* **286**, 2309 (1999).
- [7] G. E. Stedman, *Rep. Prog. Phys.* **60**, 615 (1997).
- [8] D. M. Stamper-Kurn, M. R. Andrews, A. P. Chikkatur, S. Inouye, H.-J. Miesner, J. Stenger, and W. Ketterle, *Phys. Rev. Lett.* **80**, 2027 (1998).
- [9] S. Inouye, R. F. Löw, S. Gupta, T. Pfau, A. Görlitz, T. L. Gustavson, D. E. Pritchard, and W. Ketterle, *Amplification of light and atoms in a Bose-Einstein condensate* (2000), preprint cond-mat/0006455; *Phys. Rev. Lett.*, in print.

- [10] L. V. Hau, S. E. Harris, Z. Dutton, and C. H. Behroozi, *Nature* **397**, 594 (1999).
- [11] A. P. Chikkatur, A. Görlitz, D. M. Stamper-Kurn, S. Inouye, S. Gupta, and W. Ketterle, *Phys. Rev. Lett.* **85**, 483 (2000).
- [12] R. Onofrio, C. Raman, J. M. Vogels, J. Abo-Shaeer, A. P. Chikkatur, and W. Ketterle, *Observation of superfluid flow in a Bose-Einstein condensed gas* (2000), preprint cond-mat/0006111; *Phys. Rev. Lett.*, in print.

ACES on the International Space Station: a progress report

Christophe Salomon
Ecole Normale Supérieure

We will present the recent developments concerning the ACES mission onboard the International Space Station. ACES (Atomic clock Ensemble in Space) is a European mission selected by ESA to fly on an express pallet in the early utilization phase of the ISS. Updates on the cold atom clock, PHARAO, on the Space Hydrogen Maser (SHM), microwave link (MWL), optical link (T2L2) and on the express pallet configuration will be presented. Finally, the interest to exchange signals between the various ultra-stable clocks onboard the ISS will be outlined. A simple optical link between PARCS, SUMO and ACES can perform this task.

Coherent Photoassociation of a Bose-Einstein Condensate

Juha Javanainen
University of Connecticut

In a process of photoassociation, two atoms and a photon combine to produce a diatomic molecule. In a Bose-Einstein condensate, but not in a thermal nondegenerate gas, it is possible to have coherent optical transients in photoassociation analogously to the transients known from quantum optics and laser spectroscopy. For instance, a counterpart of rapid adiabatic passage should facilitate a conversion of an atomic condensate into a molecular condensate by simply sweeping the frequency of the photoassociating laser. We discuss theoretically coherent optical transients in photoassociation. The focus is on the feasibility of experiments to produce a molecular condensate.

Ultracold Molecule Formation in Bose-Einstein Condensates

Dan Heinzen, R. A. Wynar, R. S. Freeland, C. Ryu, D. Comparat, E. Yesilada, and G. Xu
University of Texas

We have generated ultracold Rb_2 molecules in a dilute Bose-Einstein condensate (BEC) of Rb atoms, using stimulated Raman photoassociation. Because the atoms are at rest and the photons transfer negligible momentum, the molecules are formed almost perfectly at rest inside the atomic BEC. The linewidth of the Raman transition is as small as 1.5 KHz, and more than 10,000 times narrower than similar previous resonances observed in laser-cooled gases. As a result, we are able to measure the interactions between molecules and an atomic condensate for the first time. We will discuss these results, as well as our progress towards producing molecular condensates with this method. In addition, we will discuss our progress on a second project to search for T-violation with ultracold atoms and molecules.

New Clock Comparison Searches for Lorentz and CPT Violation

Ronald L. Walsworth, David Bear, Marc Humphrey,
Edward M. Mattison, David F. Phillips, Richard E. Stoner,
and Robert F. C. Vessot

*Harvard-Smithsonian Center for Astrophysics
Cambridge, MA 02138, U.S.A.*

Abstract. We present two new measurements constraining Lorentz and CPT violation using the $^{129}\text{Xe}/^3\text{He}$ Zeeman maser and atomic hydrogen masers. Experimental investigations of Lorentz and CPT symmetry provide important tests of the framework of the standard model of particle physics and theories of gravity. The two-species $^{129}\text{Xe}/^3\text{He}$ Zeeman maser bounds violations of Lorentz and CPT symmetry of the neutron at the 10^{-31} GeV level. Measurements with atomic hydrogen masers provide a clean limit of Lorentz and CPT symmetry violation of the proton at the 10^{-27} GeV level.

INTRODUCTION

Lorentz symmetry is a fundamental feature of modern descriptions of nature. Lorentz transformations include both spatial rotations and boosts. Therefore, experimental investigations of rotation symmetry provide important tests of the framework of the standard model of particle physics and single-metric theories of gravity [1].

In particular, the minimal $\text{SU}(3)\times\text{SU}(2)\times\text{U}(1)$ standard model successfully describes particle phenomenology, but is believed to be the low energy limit of a more fundamental theory that incorporates gravity. While the fundamental theory should remain invariant under Lorentz transformations, spontaneous symmetry-breaking could result at the level of the standard model in small violations of Lorentz invariance and CPT (symmetry under simultaneous application of Charge conjugation, Parity inversion, and Time reversal) [2].

Clock comparisons provide sensitive tests of rotation invariance and hence Lorentz symmetry by bounding the frequency variation of a given clock as its orientation changes, e.g., with respect to the fixed stars [3]. In practice, the most precise limits are obtained by comparing the frequencies of two co-located clocks as they rotate with the Earth (see Fig. 1). Atomic clocks are typically used, involving the electromagnetic signals emitted or absorbed on hyperfine or Zeeman transitions.

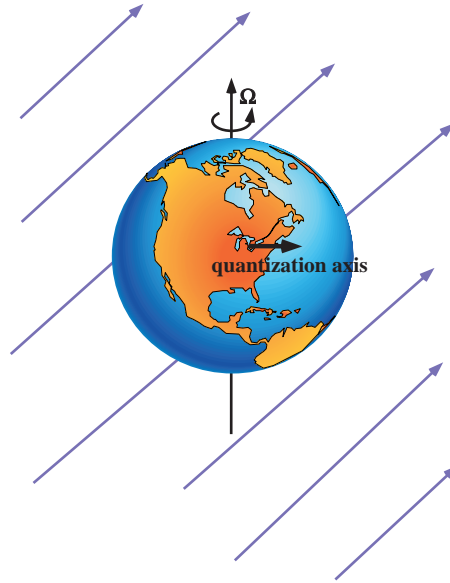


FIGURE 1. Bounds on Lorentz and CPT violation can be obtained by comparing the frequencies of clocks as they rotate with respect to the fixed stars. The standard model extension described in [3,9–17] admits Lorentz-violating couplings of noble gas nuclei and hydrogen atoms to expectation values of tensor fields. (Some of these couplings also violate CPT.) Each of the tensor fields may have an unknown magnitude and orientation in space, to be limited by experiment. The background arrows in this figure illustrate one such field.

We report results from two new atomic clock tests of Lorentz and CPT symmetry:

- (1) Using a two-species $^{129}\text{Xe}/^3\text{He}$ Zeeman maser [4–6] we placed a limit on Lorentz and CPT violation of the neutron of nearly 10^{-31} GeV, improving by more than a factor of six on the best previous measurement [7,8].
- (2) We employed atomic hydrogen masers to set an improved clean limit on Lorentz and CPT violation of the proton, at the level of nearly 10^{-27} GeV.

MOTIVATION

Our atomic clock comparisons are motivated by a standard model extension developed by Kostelecký and others [3,9–17]. This theoretical framework accommodates possible spontaneous violation of Lorentz and CPT symmetry, which may occur in a fundamental theory combining the standard model with gravity. For example, this might occur in string theory [18]. The standard model extension is quite general: it emerges as the low-energy limit of any underlying theory that generates the standard model and contains spontaneous Lorentz symmetry violation [19]. The extension retains the usual gauge structure and power-counting renormalizability of the standard model. It also has

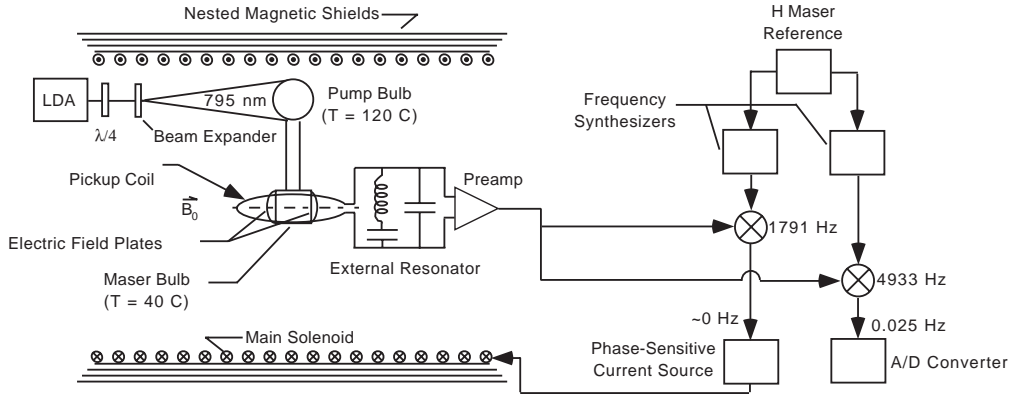


FIGURE 2. Schematic of the $^{129}\text{Xe}/^3\text{He}$ Zeeman maser

many other desirable properties, including energy-momentum conservation, observer Lorentz covariance, conventional quantization, and hermiticity. Microcausality and energy positivity are expected.

This well-motivated theoretical framework suggests that small, low-energy signals of Lorentz and CPT violation may be detectable in high-precision experiments. The dimensionless suppression factor for such effects would likely be the ratio of the low-energy scale to the Planck scale, perhaps combined with dimensionless coupling constants [3,9–19]. A key feature of the standard model extension of Kostelecký *et al.* is that it is at the level of the known elementary particles, and thus enables quantitative comparison of a wide array of tests of Lorentz symmetry. In recent work the standard model extension has been used to quantify bounds on Lorentz and CPT violation from measurements of neutral meson oscillations [9]; tests of QED in Penning traps [10]; photon birefringence in the vacuum [11,12]; baryogenesis [13]; hydrogen and antihydrogen spectroscopy [14]; experiments with muons [15]; a spin-polarized torsion pendulum [16]; observations with cosmic rays [17]; and atomic clock comparisons [3]. Recent experimental work motivated by this standard model extension includes Penning trap tests by Gabrielse *et al.* on the antiproton and H^- [20], and by Dehmelt *et al.* on the electron and positron [21,22], which place improved limits on Lorentz and CPT violation in these systems. Also, a re-analysis by Adelberger, Gundlach, Heckel, and co-workers of existing data from the “Eöt-Wash II” spin-polarized torsion pendulum [23,24] sets the most stringent bound to date on Lorentz and CPT violation of the electron: approximately 10^{-29} GeV [25].

$^{129}\text{Xe}/^3\text{He}$ MASER TEST OF LORENTZ AND CPT SYMMETRY

The design and operation of the two-species $^{129}\text{Xe}/^3\text{He}$ maser has been discussed in recent publications [4–6]. (See the schematic in Fig. 2.) Two dense, co-located ensembles of ^3He and ^{129}Xe atoms perform continuous and simultaneous maser oscillations on their respective nuclear spin 1/2 Zeeman transitions at approximately 4.9 kHz for ^3He and 1.7 kHz for ^{129}Xe in a static magnetic field of 1.5 gauss. This two-species maser operation can

be maintained indefinitely. The population inversion for both maser ensembles is created by spin exchange collisions between the noble gas atoms and optically-pumped Rb vapor [26]. The $^{129}\text{Xe}/^3\text{He}$ maser has two chambers, one acting as the spin exchange “pump bulb” and the other serving as the “maser bulb”. This two chamber configuration permits the combination of physical conditions necessary for a high flux of spin-polarized noble gas atoms into the maser bulb, while also maintaining ^3He and ^{129}Xe maser oscillations with good frequency stability: ~ 100 nHz stability is typical for measurement intervals of ~ 1 hour [6]. (A single-bulb $^{129}\text{Xe}/^3\text{He}$ maser does not provide good frequency stability because of the large Fermi contact shift of the ^{129}Xe Zeeman frequency caused by ^{129}Xe -Rb collisions [27].) Either of the noble gas species can serve as a precision magnetometer to stabilize the system’s static magnetic field, while the other species is employed as a sensitive probe for Lorentz and CPT-violating interactions or other subtle physical influences. (For example, we are also using the $^{129}\text{Xe}/^3\text{He}$ maser to search for a permanent electric dipole moment of ^{129}Xe as a test of time reversal symmetry; hence the electric field plates in Fig. 2.)

We search for a signature of Lorentz violation by monitoring the relative phases and Zeeman frequencies of the co-located ^3He and ^{129}Xe masers as the laboratory reference frame rotates with respect to the fixed stars. We operate the system with the quantization axis directed east-west on the Earth, the ^3He maser free-running, and the ^{129}Xe maser phase-locked to a signal derived from a hydrogen maser in order to stabilize the magnetic field. To leading order, the standard model extension of Kostelecký *et al.* predicts that the Lorentz-violating frequency shifts for the ^3He and ^{129}Xe maser are the same size and sign [3]. Hence the possible Lorentz-violating frequency shift in the free-running ^3He maser ($\delta\nu_{He}$) is given by:

$$\delta\nu_{He} = \delta\nu_{Lorentz} [\gamma_{He}/\gamma_{Xe} - 1], \quad (1)$$

where $\delta\nu_{Lorentz}$ is the sidereal-day-period modulation induced in both noble gas Zeeman frequencies by the Lorentz-violating interaction, and $\gamma_{He}/\gamma_{Xe} \approx 2.75$ is the ratio of gyromagnetic ratios for ^3He and ^{129}Xe .

We acquired 90 days of data for this experiment over the period April, 1999 to May, 2000. We reversed the main magnetic field of the apparatus every ~ 4 days to help distinguish possible Lorentz-violating effects from diurnal systematic variations. In addition, we carefully assessed the effectiveness of the ^{129}Xe co-magnetometer, and found that it provides excellent isolation from possible diurnally-varying ambient magnetic fields, which would not average away with field reversals. Furthermore, the relative phase between the solar and sidereal day evolved about 2π radians over the course of the experiment; hence diurnal systematic effects from any source would be reduced by averaging the results from the measurement sets.

We analyzed each day’s data and determined the amplitude and phase of a possible sidereal-day-period variation in the free-running ^3He maser frequency. (See Fig. 3 for an example of one day’s data.) We employed a linear least squares method to fit the free-running maser phase vs. time using a minimal model including: a constant (phase offset); a linear term (Larmor precession); and cosine and sine terms with sidereal day

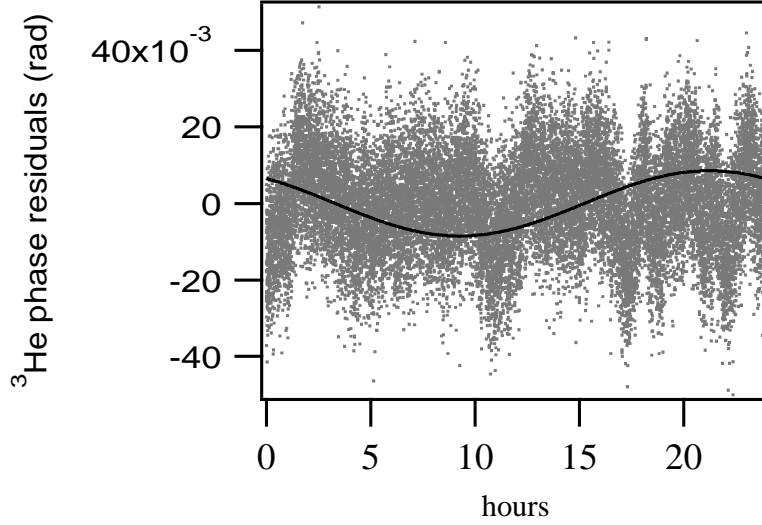


FIGURE 3. Typical data from the Lorentz/CPT test using the $^{129}\text{Xe}/^3\text{He}$ maser. ^3He maser phase data residuals are shown for one sidereal day. Larmor precession and drift terms have been removed, and the best-fit sinusoid curve (with sidereal-day-period) is displayed

period. For each day's data, we included terms corresponding to quadratic and maser amplitude-induced phase drift if they significantly improved the reduced χ^2 [28]. As a final check, we added a *faux* Lorentz-violating effect of known phase and amplitude to the raw data and performed the analysis as before. We considered our data reduction for a given sidereal day to be successful if the synthetic physics was recovered and there was no significant change in the covariance matrix generated by the fitting routine.

Using the 90 days of data, we found no statistically significant sidereal variation of the free-running ^3He maser frequency at the level of 45 nHz (one-sigma confidence). Kostelecký and Lane report that the nuclear Zeeman transitions of ^{129}Xe and ^3He are primarily sensitive to Lorentz-violating couplings of the neutron, assuming the correctness of the Schmidt model of the nuclei [3]. Thus our search for a sidereal-period frequency shift of the free-running ^3He maser ($\delta\nu_{\text{He}}$) provides a bound to the following parameters characterizing the magnitude of Lorentz/CPT violations in the standard model extension:

$$\left| -3.5\tilde{b}_J^n + 0.012\tilde{d}_J^n + 0.012\tilde{g}_{D,J}^n \right| \leq 2\pi\delta\nu_{\text{He},J} \quad ({}^{129}\text{Xe}/{}^3\text{He} \text{ maser}) \quad (2)$$

Here $J = X, Y$ denotes spatial indices in a non-rotating frame, with X and Y oriented in a plane perpendicular to the Earth's rotation axis and we have taken $\hbar = c = 1$. The parameters \tilde{b}_J^n , \tilde{d}_J^n , and $\tilde{g}_{D,J}^n$ describe the strength of Lorentz-violating couplings of the neutron to possible background tensor fields. \tilde{b}_J^n and $\tilde{g}_{D,J}^n$ correspond to couplings that violate both Lorentz and CPT symmetry, while \tilde{d}_J^n corresponds to a coupling that violates Lorentz symmetry but not CPT. All three of these parameters are different linear combinations of fundamental parameters in the underlying relativistic Lagrangian of the

standard model extension [3,9–16].

It is clear from Eqn. (2) that the $^{129}\text{Xe}/^3\text{He}$ clock comparison is primarily sensitive to Lorentz/CPT violations associated with the neutron parameter \tilde{b}_J^n . Similarly, the most precise previous search for Lorentz/CPT violations of the neutron, the $^{199}\text{Hg}/^{133}\text{Cs}$ experiment of Lamoreaux, Hunter *et al.* [7,8], also had principal sensitivity to \tilde{b}_J^n at the following level [3]:

$$\left| \frac{2}{3} \tilde{b}_J^n + \{\text{small terms}\} \right| \leq 2\pi \delta\nu_{\text{Hg},J} \quad ({}^{199}\text{Hg}/{}^{133}\text{Cs}). \quad (3)$$

In this case, the experimental limit, $\delta\nu_{\text{Hg},J}$, was a bound of 55 nHz (one-sigma confidence) on a sidereal-period variation of the ^{199}Hg nuclear Zeeman frequency, with the ^{133}Cs electronic Zeeman frequency serving as a co-magnetometer.

Therefore, in the context of the standard model extension of Kostelecký and co-workers [3], our $^{129}\text{Xe}/^3\text{He}$ maser measurement improves the constraint on \tilde{b}_J^n to nearly 10^{-31} GeV, or more than six times better than the $^{199}\text{Hg}/^{133}\text{Cs}$ clock comparison [7,8]. Note that the ratio of this limit to the neutron mass ($10^{-31}\text{GeV}/m_n \sim 10^{-31}$) compares favorably to the dimensionless suppression factor $m_n/M_{\text{Planck}} \sim 10^{-19}$ that might be expected to govern spontaneous Lorentz and CPT symmetry breaking originating at the Planck scale. We expect more than an order of magnitude improvement in sensitivity to Lorentz/CPT-violation of the neutron using a new device recently demonstrated in our laboratory: the $^{21}\text{Ne}/^3\text{He}$ Zeeman maser.

HYDROGEN MASER TEST OF LORENTZ AND CPT SYMMETRY

The hydrogen maser is an established tool in precision tests of fundamental physics [29]. Hydrogen masers operate on the $\Delta F = 1$, $\Delta m_F = 0$ hyperfine transition in the ground state of atomic hydrogen [30]. Hydrogen molecules are dissociated into atoms in an RF discharge, and the atoms are state selected via a hexapole magnet (Fig. 4). The high field seeking states, ($F = 1$, $m_F = +1, 0$) are focused into a Teflon coated cell which resides in a microwave cavity resonant with the $\Delta F = 1$ transition at 1420 MHz. The $F = 1$, $m_F = 0$ atoms are stimulated to make a transition to the $F = 0$ state by the field of the cavity. A static magnetic field of ~ 1 milligauss is applied to maintain the quantization axis of the H atoms.

The hydrogen transitions most sensitive to potential Lorentz and CPT violations are the $F = 1$, $\Delta m_F = \pm 1$ Zeeman transitions. In the 0.6 mG static field applied for these measurements, the Zeeman frequency is $\nu_Z \approx 850$ Hz. We utilize a double resonance technique to measure this frequency with a precision of ~ 1 mHz [31]. We apply a weak magnetic field perpendicular to the static field and oscillating at a frequency close to the Zeeman transition. This audio-frequency driving field couples the three sublevels of the $F = 1$ manifold of the H atoms. Provided a population difference exists between the $m_F = \pm 1$ states, the energy of the $m_F = 0$ state is altered by this coupling, thus shifting the measured maser frequency in a carefully analyzed manner [31] described

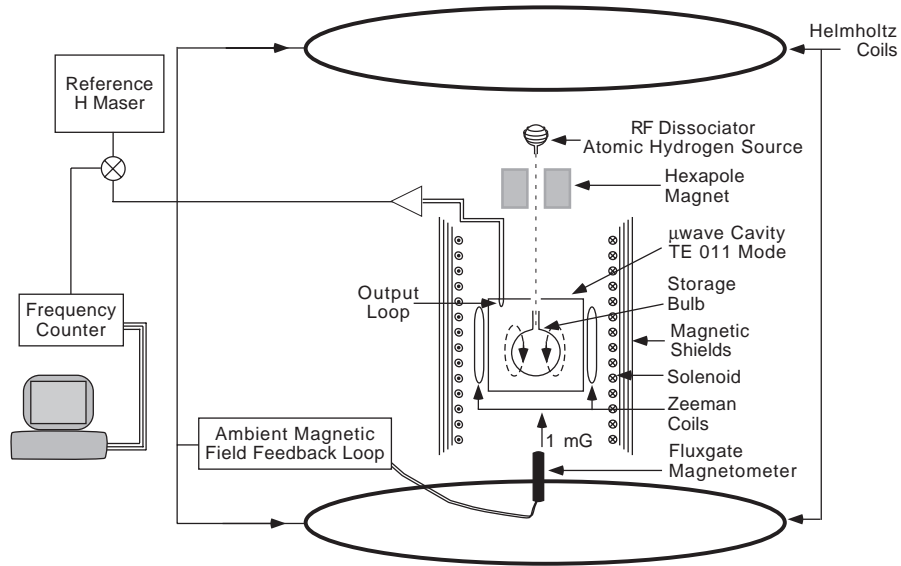


FIGURE 4. Schematic of the H maser in its ambient field stabilization loop.

by a dispersive shape (Fig. 5(a)). Importantly, the maser frequency is unchanged when the driving field is exactly equal to the Zeeman frequency. Therefore, we determine the Zeeman frequency by measuring the driving field frequency at which the maser frequency in the presence of the driving field is equal to the unperturbed maser frequency.

The $F = 1$, $\Delta m_F = \pm 1$ Zeeman frequency is directly proportional to the static magnetic field, in the small-field limit. Four layers of high permeability (μ -metal) magnetic shields surround the maser (Fig. 4), screening external field fluctuations by a factor of 32 000. Nevertheless, external magnetic field fluctuations cause remnant variations in the observed Zeeman frequency. As low frequency magnetic noise in the neighborhood of this experiment is much larger during the day than late at night, the measured Zeeman frequency could be preferentially shifted by this noise (at levels up to ~ 0.5 Hz) with a 24 hour periodicity which is difficult to distinguish from a true sidereal signal in our relatively short data sample. Therefore, we employ an active stabilization system to cancel such magnetic field fluctuations (Fig. 4). A fluxgate magnetometer placed as close to the maser cavity as possible controls large (2.4 m dia.) Helmholtz coils surrounding the maser via a feedback loop to maintain a constant ambient field. This feedback loop reduces the fluctuations at the sidereal frequency to below the equivalent of $1 \mu\text{Hz}$ on the Zeeman frequency at the location of the magnetometer.

The Zeeman frequency of a hydrogen maser was measured for 32 days over the period Nov., 1999 to March, 2000. During data taking, the maser remained in a closed, temperature controlled room to reduce potential systematics from thermal drifts which might be expected to have 24 hour periodicities. The feedback system also maintained a constant ambient magnetic field. Each Zeeman measurement took approximately 20 minutes to acquire and was subsequently fit to extract a Zeeman frequency (Fig. 5(a)). Also mon-

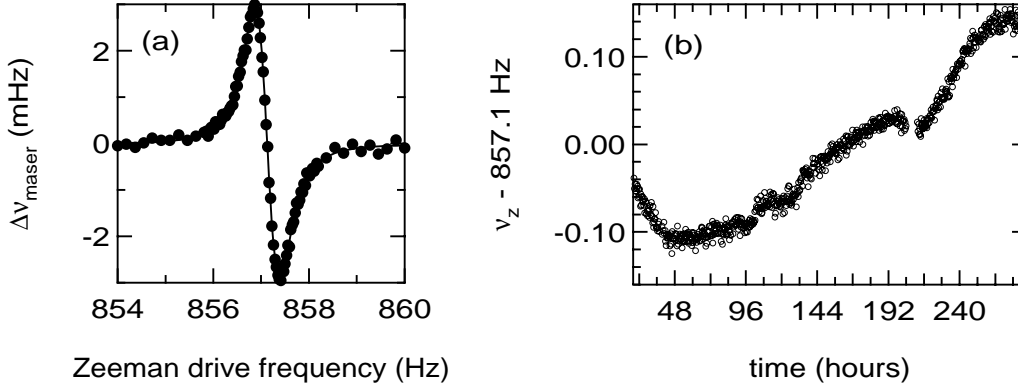


FIGURE 5. (a) An example of a double resonance measurement of the $F = 1$, $\Delta m_F = \pm 1$ Zeeman frequency in the hydrogen maser. The change from the unperturbed maser frequency is plotted versus the driving field frequency. (b) Zeeman frequency data from 11 days of the Lorentz/CPT test using the H maser.

itored were maser amplitude, residual magnetic field fluctuation, ambient temperature, and current through the solenoidal coil which determines the Zeeman frequency (Fig. 4).

The data were then fit to extract the sidereal-period sinusoidal variation of the Zeeman frequency. (See Fig. 5(b) for an example of 11 days of data.) In addition to the sinusoid, piecewise linear terms (whose slopes were allowed to vary independently for each day) were used to model the slow remnant drift of the Zeeman frequency. No significant sidereal-day-period variation of the hydrogen $F = 1$, $\Delta m_F = \pm 1$ Zeeman frequency was observed. Our measurements set a bound on the magnitude of such a variation of $\delta\nu_Z^H \leq 0.34$ mHz (one-sigma level). Expressed in terms of energy, this is a shift in the Zeeman splitting of about $1 \cdot 10^{-27}$ GeV.

The hydrogen atom is directly sensitive to Lorentz and CPT violations of the proton and the electron. Following the notation of reference [14], one finds that a limit on a sidereal-day-period modulation of the Zeeman frequency ($\delta\nu_Z^H$) provides a bound to the following parameters characterizing the magnitude of Lorentz/CPT violations in the standard model extension of Kostelecký and co-workers:

$$|b_3^e + b_3^p - d_{30}^e m_e - d_{30}^p m_p - H_{12}^e - H_{12}^p| \leq 2\pi\delta\nu_Z^H \quad (4)$$

for the low static magnetic fields at which we operate. (Again, we have taken $\hbar = c = 1$.) The terms b^e and b^p describe the strength of background tensor field couplings that violate Lorentz and CPT symmetry while the H and d terms describe couplings that violate Lorentz symmetry but not CPT [14]. The subscript 3 in Eqn. (4) indicates the direction along the quantization axis of the apparatus, which is vertical in the lab frame but rotates with respect to the fixed stars with the period of the sidereal day.

As in refs. [3,21], we can re-express the time varying change in the hydrogen Zeeman frequency in terms of parameters expressed in a non-rotating frame as

$$2\pi\delta\nu_{Z,J}^H = (\tilde{b}_J^p + \tilde{b}_J^e) \sin \chi. \quad (5)$$

where $\tilde{b}_J^w = b_J^w - d_{j0}^w m_w - \frac{1}{2}\epsilon_{JKL} H_{KL}^w$, $J = X, Y$ refers to non-rotating spatial indices in the plane perpendicular to the rotation vector of the earth, w refers to either the proton or electron parameters, and $\chi = 48^\circ$ is the co-latitude of the experiment.

As noted above, a re-analysis by Adelberger, Gundlach, Heckel, and co-workers of existing data from the ‘‘Eöt-Wash II’’ spin-polarized torsion pendulum [23,24] sets the most stringent bound to date on Lorentz and CPT violation of the electron: $\tilde{b}_J^e \leq 10^{-29}$ GeV [25]. Therefore, in the context of the standard model extension of Kostelecký and co-workers [14,3] the H maser measurement to date constrains Lorentz and CPT violations of the proton parameter $\tilde{b}_J^p \leq 2 \cdot 10^{-27}$ GeV at the one sigma level. This limit is comparable to that derived from the $^{199}\text{Hg}/^{133}\text{Cs}$ experiment of Lamoreaux, Hunter *et al.* [7,8] but in a much cleaner system (the hydrogen atom nucleus is a proton, compared to the complicated nuclei of ^{199}Hg and ^{133}Cs).

CONCLUSIONS

Precision comparisons of atomic clocks provide sensitive tests of Lorentz and CPT symmetries, thereby probing extensions to the standard model [3,9–17] in which these symmetries can be spontaneously broken. Measurements using the two-species $^{129}\text{Xe}/^3\text{He}$ Zeeman maser constrain violations of Lorentz and CPT symmetry of the neutron at the 10^{-31} GeV level. Measurements with atomic hydrogen masers provide clean tests of Lorentz and CPT symmetry violation of the proton at the 10^{-27} GeV level. Improvements in both experiments are being pursued.

ACKNOWLEDGMENTS

We gratefully acknowledge the encouragement and active support of these projects by Alan Kostelecký, and technical assistance by Marc Rosenberry and Timothy Chupp. Development of the $^{129}\text{Xe}/^3\text{He}$ Zeeman maser was supported by a NIST Precision Measurement Grant. Support for the Lorentz violation tests was provided by NASA grant NAG8-1434.

REFERENCES

1. Will, C.M., *Theory and Experiment in Gravitational Physics*, Cambridge University Press, New York, 1981.
2. The discrete symmetries C, P, and T are discussed, for example, in Sachs, R.G., *The Physics of Time Reversal*, University of Chicago, Chicago, 1987.
3. Kostelecký, V.A., and Lane, C.D., *Phys. Rev. D* **60**, 116010/1-17 (1999).
4. Chupp, T.E., Hoare, R.J., Walsworth, R.L., and Wu, B., *Phys. Rev. Lett.* **72**, 2363-2366 (1994).

5. Stoner, R.E., Rosenberry, M.A., Wright, J.T., Chupp, T.E., Oteiza, E.R., and Walsworth, R.L., *Phys. Rev. Lett.* **77**, 3971-3974 (1996).
6. Bear, D., Chupp, T.E., Cooper, K., DeDeo, S., Rosenberry, M.A., Stoner, R.E., and Walsworth, R.L., *Phys. Rev. A* **57**, 5006-5008 (1998).
7. Berglund, C.J., Hunter, L.R., Krause, Jr., D., Prigge, E.O., Ronfeldt M.S., and Lamoreaux, S.K., *Phys. Rev. Lett.* **75**, 1879-1882 (1995).
8. Hunter, L.R., Berglund, C.J., Ronfeldt, M.S., Prigge, E.O., Krause, D., and Lamoreaux, S.K., "A Test of Local Lorentz Invariance Using Hg and Cs Magnetometers," in *CPT and Lorentz Symmetry*, edited by Kostelecký, V.A., World Scientific, Singapore, 1999, pp. 180-186.
9. Kostelecký, V.A., and Potting, R., "CPT, Strings, and the $K - \bar{K}$ System," in *Gamma Ray-Neutrino Cosmology and Planck Scale Physics*, edited by Cline, D.B., World Scientific, Singapore, 1993, hep-th/9211116; *Phys. Rev. D* **51**, 3923-3935 (1995); Colladay D., and Kostelecký, V.A., *Phys. Lett. B* **344**, 259-265 (1995); *Phys. Rev. D* **52**, 6224-6230 (1995); Kostelecký, V.A., and Van Kooten, R., *Phys. Rev. D* **54**, 5585 (1996); Kostelecký, V.A., *Phys. Rev. Lett.* **80**, 1818-1821 (1998); *Phys. Rev. D* **61**, 16002/1-9 (2000).
10. Bluhm, R., Kostelecký, V.A., and Russell, N., *Phys. Rev. Lett.* **79**, 1432-1435 (1997); *Phys. Rev. D* **57**, 3932-3943 (1998).
11. Carroll, S.M., Field, G.B., and Jackiw, R., *Phys. Rev. D* **41**, 1231-1240 (1990).
12. Colladay, D., and Kostelecký, V.A., *Phys. Rev. D* **55**, 6760-6774 (1997); *ibid.* **58**, 116002/1-23 (1998); Jackiw, R., and Kostelecký, V.A., *Phys. Rev. Lett.* **82**, 3572-3575 (1999);
13. Bertolami, O., Colladay, D., Kostelecký, V.A., and Potting, R., *Phys. Lett. B* **395**, 178-183 (1997).
14. Bluhm, R., Kostelecký, V.A., and Russell, N., *Phys. Rev. Lett.* **82**, 2254-2257 (1999).
15. Bluhm, R., Kostelecký, V.A., and Lane, C.D., *Phys. Rev. Lett.* **84**, 1098-1101 (2000).
16. Bluhm, R. and Kostelecký, V.A., *Phys. Rev. Lett.* **84**, 1381-1384 (2000).
17. Coleman, S., and Glashow, S.L., *Phys. Rev. D* **56**, 116008/1-14 (1999).
18. Kostelecký, V.A. and Samuel, S., *Phys. Rev. D* **39**, 683-685 (1989); *ibid.* **40**, 1886-1903 (1989); Kostelecký, V.A. and Potting, R., *Nucl. Phys. B* **359**, 545-570 (1991); *Phys. Lett. B* **381**, 89-96 (1996).
19. Kostelecký, V.A., and Samuel, S., *Phys. Rev. Lett.* **63**, 224-227 (1989); *ibid.* **66**, 1811-1814 (1991).
20. Gabrielse, G., Khabbaz, A., Hall, D.S., Heimenn, C., Kalinowski, H., and Jhe, W., *Phys. Rev. Lett.* **82**, 3198-3201 (1999).
21. Mittleman, R.K., Ioannou, I.I., Dehmelt, H.G., and Russell, N., *Phys. Rev. Lett.* **83**, 2116-2119 (1999).
22. Dehmelt, H., Mittleman, R., Van Dyck, Jr., R.S., and Schwinberg, P., *Phys. Rev. Lett.* **83**, 4694-4696 (1999).
23. Adelberger, E.G., *et al.*, in *Physics Beyond the Standard Model*, edited by P. Herczeg *et al.*, World Scientific, Singapore, 1999, p. 717.
24. Harris, M.G., Ph.D. thesis, Univ. of Washington, 1998.
25. Heckel, B., presented at International Conference on Orbis Scientiae 1999: Quantum Gravity, Generalized Theory of Gravitation and Superstring Theory Based Unification (28th Conference on High Energy Physics and Cosmology Since 1964), Fort Lauderdale, Florida, 16-19 Dec., 1999.
26. Walker, T.G., and Happer, W., *Rev. Mod. Phys.* **69**, 629-642 (1997).

27. Romalis, M.V., and Cates, G.D., *Phys. Rev. A* **58**, 3004-3011 (1998); Newbury, N.R., Barton, A.S., Bogorad, P., Cates, G.D., Mabuchi, H., and Saam, B., *Phys. Rev. A* **48**, 558-568 (1993); Schafer, S.R., Cates, G.D., Chien, T.R., Gonatas, D., Happer, W., and Walker, T.G., *Phys. Rev. A* **39**, 5613-5623 (1989).
28. We employed the F-test at the 99% confidence level to decide whether the addition of a new term to the fit model was justified. See Philip R. Bevington, *Data Reduction and Error Analysis for the Physical Sciences, Second Ed.*, McGraw-Hill, Boston, 1992, ch. 11.
29. Vessot, R.F.C., *et al.*, *Phys. Rev. Lett.* **45**, 2081-2084 (1980); Turneaure, R.J.P., Will, C.M., Farrell, B.F., Mattison, E.M., and Vessot, R.F.C., *Phys. Rev. D* **27**, 1705-1714 (1983); Walsworth, R.L., Silvera, I.F., Mattison, E.M., and Vessot, R.F.C., *Phys. Rev. Lett.* **64**, 2599-2602 (1990).
30. Kleppner, D., Goldenberg, H.M., and Ramsey, N.F., *Phys. Rev.* **126**, 603-615 (1962); Kleppner, D., Berg, H.C., Crampton, S.B., Ramsey, N.F., Vessot, R.F.C., Peters, H.E., and Vanier, J., *Phys. Rev.* **138**, A972-983 (1965).
31. Andresen, H.G., *Z. Physik*, **210**, 113-141 (1968).

CLOCK TECHNOLOGY DEVELOPMENT FOR THE LASER COOLING AND ATOMIC PHYSICS (LCAP) PROGRAM

D.J. Seidel, W.M. Klipstein, R.J. Thompson, J. Kohel, and L. Maleki, Jet Propulsion Laboratory, California Institute of Technology, Pasadena, California, 91109

Mailing address: D.J. Seidel, MS 298/100, Jet Propulsion Laboratory, 4800 Oak Grove Drive, Pasadena, California 91109, U.S.A.

Abstract. In this paper we present an overview of the present and future of the Laser Cooling and Atomic Physics (LCAP) program in support of NASA's Micro-gravity Fundamental Physics program. We address the role played by the Jet Propulsion Laboratory in developing the core technologies to support the wide variety of science that we envision will be explored by this program. We also discuss the various science platforms available on the ISS and the challenges of performing a laser cooled atomic clock experiment in this environment.

INTRODUCTION

NASA's Fundamental Physics program has identified Laser Cooling and Atomic Physics (LCAP) as one of three disciplines (along with low-temperature and gravitational physics) which are poised to take advantage of the microgravity environment offered by the ISS and the Space Shuttle. Two clock experiments have been selected by NASA for flight aboard the International Space Station (ISS): the Primary Atomic Reference Clock in Space (PARCS), with principle investigators at the National Institute of Standards and Technology (NIST) and the University of Colorado; and the Rubidium Atomic Clock Experiment (RACE), with principle investigator at Yale University. In addition, 11 ground-based investigations have been funded to date on topics including atomic clocks, Bose-Einstein Condensation (BEC), Electric Dipole Moment (EDM) searches, and atom interferometry.

The Time and Frequency Sciences and Technology Group at the Jet Propulsion Laboratory plays a key role in this program, supporting LCAP missions through the design, construction and integration of instruments capable of meeting the science goals. Ground testbeds in our laboratory are used to refine our designs and aid in the development of new technologies required for the flight missions.

CLOCK EXPERIMENTS

Two clock experiments will form the first generation of LCAP flight projects. Each will rely on microgravity for their performance and, in addition, will utilize the difference in the gravitational potential between the earth's surface and the International Space Station to perform a variety of tests of the theory of general relativity. The first of these, the Primary Atomic Reference Clock in Space, (PARCS) has as Co-Principle Investigators Dr. Don Sullivan of the National Institute of Standards and Technology (NIST), and Professor Neil Ashby of the University of Colorado. PARCS is planned to fly aboard the space station late in 2004. The other flight experiment, the Rubidium Atomic Clock Experiment (RACE), is led by Principle Investigator Kurt Gibble, of Yale University. This experiment differs from the PARCS experiment in that it utilizes a different atomic species (rubidium as opposed to cesium) which can result in improved time accuracy. Both experiments are currently being designed to fly in an EXPRESS rack, with a link to an external GPS receiver for use in time transfer.

A generic schematic of a space-based atomic clock is shown in figure 1. A cold sample of atoms is collected in the source region and then given a push so that it drifts freely along the beam tube. The atoms pass into a state selection chamber, which prepares them in a particular state, and then through a microwave interrogation chamber which induces a particular atomic transition, if the frequency of the microwaves is

exactly that of the atoms. The final state of the atoms is then read out by lasers as they pass through the detection region. A more detailed discussion of space based clocks can be found in the papers by Sullivan *et al.* and Gibble *et al.* in these proceedings.

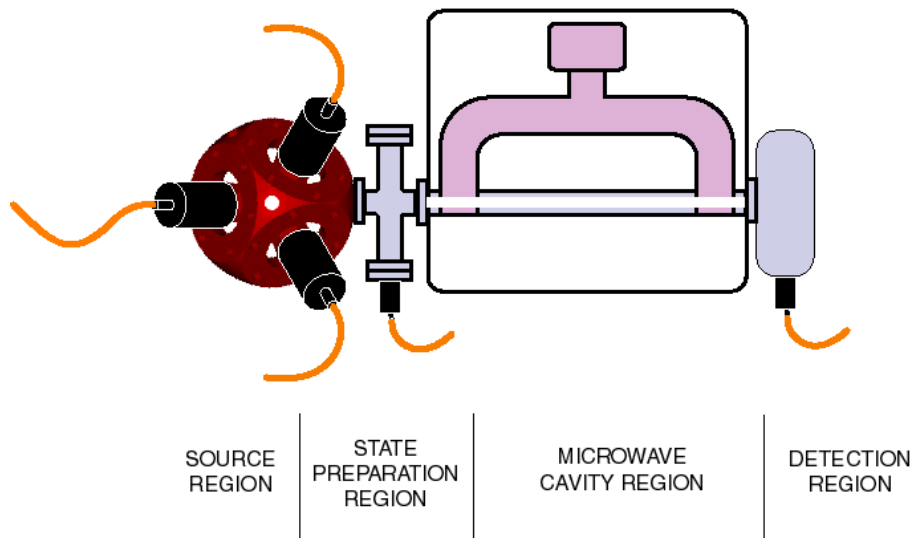


FIGURE 1. Schematic of laser-cooled space clock.

INSTRUMENT DEVELOPMENT

Instrument development and PI support for both of the current flight projects and for later LCAP flights is provided by the Time and Frequency Sciences and Technology Group of the Jet Propulsion Laboratory. Work in our ground test bed has focused initially on demonstrating the feasibility of performing laser

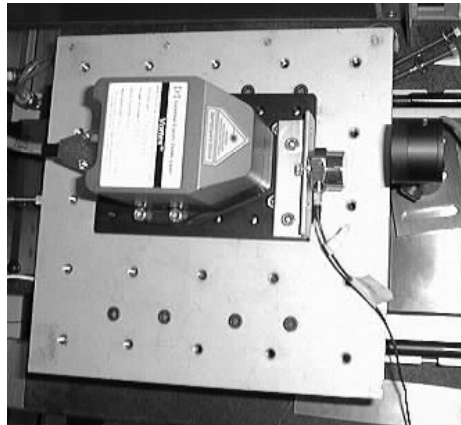


Figure 2 New Focus Vortex laser on miniature shake table. The laser performed well in our tests.

cooling experiments in space. Here the challenges are to dramatically reduce the volume and mass requirements of a typical laser-cooling experiment, while improving the reliability and ruggedness of the apparatus so as to be capable of surviving a typical launch, and then of operating for several months of stand-alone operation. We have achieved temperatures below $7\ \mu\text{K}$ for a cloud of Cesium atoms in our test-bed laser cooling apparatus, using laser and optical components that appear suitable for a space application (in terms of mass, power, and volume).

One of the most challenging technologies is the development of rugged compact laser systems, capable of producing high power single frequency laser light with the stability and frequency tunability needed to meet the demands of a laser cooling experiment. We have vibration tested a variety of optical components that will be included in the PARCS laser system up to the qualification level required for a shuttle launch (see figure 2). We have also demonstrated a compact laser system built within the mass and volume constraints of the PARCS mission. Our current baseline laser system for PARCS will have a single master laser that will then be used to injection lock two slave lasers. Acousto-optical modulators positioned between the master and slave laser allow one to have a very fine control of the laser frequency, while similar modulators following the slave laser allow the laser intensity to be controlled as well.

Another example of the unique technologies being developed at JPL is the novel non-magnetic shutter system shown in figure 3, which is capable of performing reliably for one year in ultra-high vacuum, without perturbing the microgravity environment.

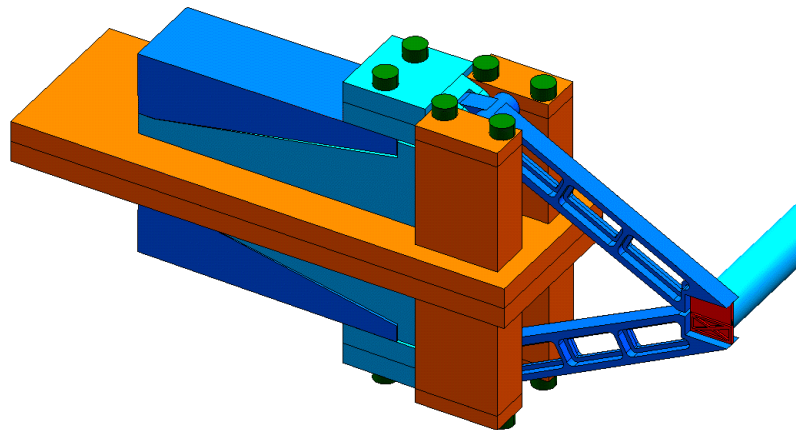


FIGURE 3 . Conceptual design of non-magnetic shutter for the PARCS and RACE missions.

Other components and subsystems are also under development to provide ISS experimenters with the same capability currently available in ground-based laboratories. These include ultra-high vacuum systems, and oven sources of alkali atoms. Future developments will likely include cold atomic beams, compact magnetic traps, and laser systems for driving Raman transitions in Cesium atoms (these latter would be required for an atom interferometer experiment or one involving Raman cooling).

A key to minimizing the overall cost of the LCAP program is to develop experiments with as much modularity and reusability as possible. Thus the laser and optics subassembly for the PARCS experiment will also be suitable for a variety of future LCAP flights using atomic cesium. The RACE laser and optics subassembly, will have a similar design to the PARCS one, but will utilize different components in order to match the rubidium wavelength. Again, this system will be designed to be easily refurbished for future flights involving rubidium. Currently it is believed that most, if not all, LCAP flights will utilize one of these atomic species.

AVAILABLE SCIENCE PLATFORMS ON THE ISS

The ISS carries a number of different platforms for science payloads, distinguished first and foremost by those interior to the station and those exterior. The various platforms provide different allocations of volume, power, and environmental control. For the two flight projects, we have studied three possible platforms: the EXPRESS pallet, a platform mounted external to the station, an EXPRESS rack, which is an internal platform, and the Fluids Interface Rack (FIR), a component of the Fluids and Combustion facility that may have available space. We are currently baselining the EXPRESS Racks, shown in Fig. 4, utilizing the Active Rack Isolation System (ARIS) inside the U.S. Laboratory Module, as our preferred platform. Only in the ARIS systems will the Station provide a true microgravity vibratory environment, which is required for our experiment (the FIR also provides this capability and appears to be a suitable backup choice). By carefully reviewing the capabilities available on the various science platforms we are able to design our instruments to operate within the available envelopes, so while launch lies far in the future, these issues must be addressed in the earliest stages of the project. Beyond the obvious issues of mass, volume and power available, we must also consider the appropriate orientation of the clock cavity with respect to the direction of travel of the space station, in order to minimize the impact of quasi-steady accelerations. A further issue for the two clock missions arises from the need to compare the space clocks with the best earth-based clocks. This will be accomplished via GPS carrier phase frequency transfer, which will require an external GPS receiver and a high quality rf or fiber optic link between the interior and exterior of the station.

SUMMARY

Laser Cooling and Atomic Physics is an exciting new area for fundamental physics research in microgravity. Two flight projects, both involving ultra-precise atomic clocks, are currently planned to fly aboard the Space Station, the first in 2004, and the second in 2006. Key technologies being developed by the Jet Propulsion Laboratory for the current flight projects should also support a wide range of possible future missions, which we envision will be launched every two years.

ACKNOWLEDGEMENTS

This work was carried out by the Jet Propulsion Laboratory, California Institute of Technology, under a contract with the National Aeronautics and Space Administration. We acknowledge many fruitful discussions with Don Sullivan, Leo Hollberg, Steve Jefferts, John Kitching, Hugh Robinson, Fred Walls, Tom Heavner, Tom Parker, and Dawn Meekhof of NIST, with Andrea De Marchi of Politecnico di Torino, with Neil Ashby of the University of Colorado, and with Kurt Gibble of Yale University. The picture of the PARCS/RACE shutter was produced by Fabien Nicaise of JPL.